



HAL
open science

Hydrophobised carbon foams for improved long-term seasonal solar thermal energy storage

P. Jana, E. Palomo del Barrio, M. Dubois, M. Duquesne, A. Godin, Christine Vautrin-UI, V. Fierro, G. Medjahdi, A. Celzard

► **To cite this version:**

P. Jana, E. Palomo del Barrio, M. Dubois, M. Duquesne, A. Godin, et al.. Hydrophobised carbon foams for improved long-term seasonal solar thermal energy storage. *Solar Energy Materials and Solar Cells*, 2021, 220, pp.110849. 10.1016/j.solmat.2020.110849 . hal-03145580

HAL Id: hal-03145580

<https://uca.hal.science/hal-03145580v1>

Submitted on 17 Oct 2021

HAL is a multi-disciplinary open access archive for the deposit and dissemination of scientific research documents, whether they are published or not. The documents may come from teaching and research institutions in France or abroad, or from public or private research centers.

L'archive ouverte pluridisciplinaire **HAL**, est destinée au dépôt et à la diffusion de documents scientifiques de niveau recherche, publiés ou non, émanant des établissements d'enseignement et de recherche français ou étrangers, des laboratoires publics ou privés.

Hydrophobised carbon foams for improved long-term seasonal solar thermal energy storage

P. Jana¹, E. Palomo del Barrio^{2,3}, M. Dubois⁴, M. Duquesne⁵, A. Godin⁵, C. Vautrin-UI⁶, V. Fierro¹, G. Medjahdi¹, A. Celzard^{1*}

¹ Université de Lorraine, CNRS, IJL, 88000 Epinal, France

² Centre for Cooperative Research on Alternative Energies (CIC energiGUNE), Basque Research and Technology Alliance (BRTA), Alava Technology Park, Albert Einstein 48, 01510 Vitoria-Gasteiz, Spain

³ Ikerbasque, Basque Foundation for Science, María Díaz de Haro 3, 48013 Bilbao, Spain

⁴ Institut de Chimie de Clermont-Ferrand (ICCF), Université Blaise Pascal, UMR CNRS 6296, 63177 Aubière Cedex, France

⁵ Bordeaux INP, CNRS, I2M Bordeaux, ENSCBP, 16 avenue Pey Berland, 33607 Pessac Cedex, France

⁶ Interfaces, Confinement, Matériaux et Nanostructures – UMR CNRS 7374, 1b rue de la Férollerie, CS 40059, 45071 Orléans cedex 2, France

* Corresponding author. Tel: + 33 372 74 96 14. Fax: + 33 372 74 96 38. E-mail address :

Alain.Celzard@univ-lorraine.fr (A. Celzard)

Abstract

Composites carbon foams based on sucrose-based char matrix and graphite filler were prepared and characterised with the aim of hosting sugar alcohols as phase-change materials (PCMs) in the context of thermal energy storage (TES). Seasonal solar TES demands an excellent undercooling of the molten PCM infiltrated in the foam, so that the heat can be stored as long as possible. The present paper demonstrates how the surface of such composite foams, i.e., comprising two carbon phases of different reactivities, can be modified for promoting undercooling. For that purpose, 8 different hydrophobisation treatments were applied, and the results were compared with those of the non-treated foam, in which heterogeneous nucleation could not be avoided. We show that one kind of functionalisation was successful, i.e., it fully preserved the melting point and the enthalpy of melting of the hosted phase-change material and completely avoided the heterogeneous nucleation of the PCM, while maintaining the thermal conductivity in the range required for this kind of application.

Keywords: Seasonal thermal heat storage; Sugar alcohols; Carbon matrix; Hydrophobisation; Subcooling; Heterogeneous nucleation

1. Introduction

Despite a significant number of researches all over the past decades, storing efficiently solar thermal energy is still challenging. Most commercially available systems are indeed based on sensible heat storage technologies, which usually provide very low energy density, especially in applications where heat is stored over a narrow range of temperature. Latent heat storage based on phase-change materials (PCMs) offers the opportunity to overcome such drawback. Indeed, PCMs are able to absorb heat upon melting, and delivering it back upon crystallisation, at almost constant temperature and they provide energy density five to ten times higher than that of sensible heat storage [1-4]. However, the thermal conductivity of PCMs is most of the time too low, thus leading to heat exchangers oversizing and reduction of the efficacy of the systems, especially when the temperature of the heat transfer fluid is close to the melting/crystallisation point of the PCM, as it is the case of solar thermal energy storage (STES) applied to the building sector [5-7]. Besides using finned heat exchangers, heat transfer enhancement in PCM-based storage technologies can also be achieved by other ways [8-11], among them the encapsulation of PCMs, either in small spheres suspended in the heat transfer fluid, or in highly conducting porous matrices in close contact with the heat exchanger. The second option has been widely investigated, and various materials mainly based on graphitic porous structures have been developed [9,12-18].

The problem becomes more complex when seasonal STES is considered. Unlike most heat storage applications, for which the storage time is short (typically less than one day), seasonal storage near room temperature is expected to work over periods of several weeks to several months and therefore requires additional conditions for being efficient. PCMs are only useful for STES if it can be guaranteed that the PCM does not crystallise spontaneously during the storage period, which would lead to loss of the charge prior to use. This can be achieved by

sizing the thermal insulation to prevent the temperature of the PCM from falling below its melting point. However, this solution entails unaffordable costs. An attractive alternative to oversized thermal insulation consists in using PCMs with very low probability of homogeneous nucleation. Obviously, heterogeneous nucleation must be avoided too; thus, solutions of heat transfer enhancement promoting such a phenomenon should be discarded. If these conditions are fulfilled, it is therefore expected that the heat can be stored for quite long times in undercooled PCMs, and might be recovered at the desired moment by any perturbation of the system such as mechanical or thermal shock [19-23].

Seasonal STES based on the use of sugar alcohols as PCMs was shown to be particularly relevant, since the latter combine highly valuable properties such as low cost, availability and natural origin, absence of toxicity and of corrosive character, high energy density (130 – 200 kWh m⁻³), rather low melting points (typically in the range 70 – 120°C), and significant but stable undercooling [24,25 and refs. therein].

Whether used pure or as eutectic mixtures for getting PCMs, sugar alcohols such as xylitol, sorbitol, erythritol and mannitol, among others, are highly polar molecules. Therefore, their encapsulation in porous carbonaceous hosts of low surface energy should prevent the nucleation of crystallites and hence favour undercooling. Therefore, storing energy at temperatures far below the melting point should be possible for long periods, thus reducing thermal losses. In a recent work, composite carbon foams made of sucrose coke as matrix and natural graphite flakes as filler were produced and shown to meet all aforementioned prerequisites for seasonal STES after impregnation by sugar alcohols used as PCMs [26]. Our group indeed demonstrated that, depending both on the requirements of the application (e.g. delivered power, temperature, operating conditions during heat delivery) and on the nature of the sugar alcohol, carbon foams having at the same time high open porosity (typically higher

than 80%), moderate thermal conductivity (typically from 3 to 8 W m⁻¹ K⁻¹) and affordable cost (less than 6 €/kg) were needed. We showed in the same work how to fulfil such antagonistic properties using experimental design and related modelling (analysis of variance and response surface analysis) in order to find the optimum formulation. However, no experiments had been published proving the efficiency as such carbon foams as hosts for sugar alcohols for seasonal STES. These PCMs indeed have a low thermal conductivity in the solid state, typically 0.3 – 1.3 W m⁻¹ K⁻¹ [25], and still the proof of concept was missing. Furthermore, no surface treatment had been performed for making them more hydrophobic than they actually were, with the goal of observing a beneficial effect on long-term undercooling after heat storage.

The present paper thus aims at evaluating the aforementioned optimised carbon foams as conductive porous hosts for seasonal STES based on sugar alcohols. These carbon materials were tested as such as a reference and, after various hydrophobisation treatments, their efficiency in terms of delivered power upon heat discharge and undercooling was evaluated. We show that grafting fluorine atoms or depositing silica onto a carbonaceous surface is an efficient route to increase its hydrophobic character and prevent heterogeneous PCM nucleation, thus promoting longer heat storage. The most promising sugar alcohols for seasonal STES, namely erythritol, xylitol and, more specifically, their eutectic mixture [24, 25], are used in this work. Not only do they have a melting point suitable for seasonal STES and a high latent heat of melting, but also, unlike many other sugar alcohols, they have fairly good thermal stability [27-29].

2. Materials and methods

2.1 Preparation of carbon foams

The synthesis and properties of carbon foams having both porous structure and thermal conductivity optimised for being used as hosts for sugar alcohols have been thoroughly described elsewhere [26]. However, it is useful to recall here that such materials were prepared by dissolving sucrose and suspending natural graphite flakes in an aqueous solution of nickel nitrate. After homogenisation, the resultant blend was heated for 2 days in a ventilated oven at 120°C. During this step, polycondensation of sucrose catalysed by the metal salt occurred, the result of which was the release of water vapour and the production of rigid foam. After stabilisation of the latter, pyrolysis was carried out at 900°C in nitrogen flow, leading to a composite (sucrose char / graphite particles) carbon foam. It was shown that nickel behaved as a catalyst for both foaming and subsequent partial graphitisation. Catalytic graphitisation was required for further improving the thermal conductivity, which was not possible by adding more graphite filler since the latter reduced the final porosity. Finding the delicate compromise leading to the optimal amount of each compound therefore required the use of experimental design and the statistical analysis of the results. Fig. 1 shows a few samples having open porosity and thermal conductivity of 85.8% and 3.1 W m⁻¹ K⁻¹, respectively.

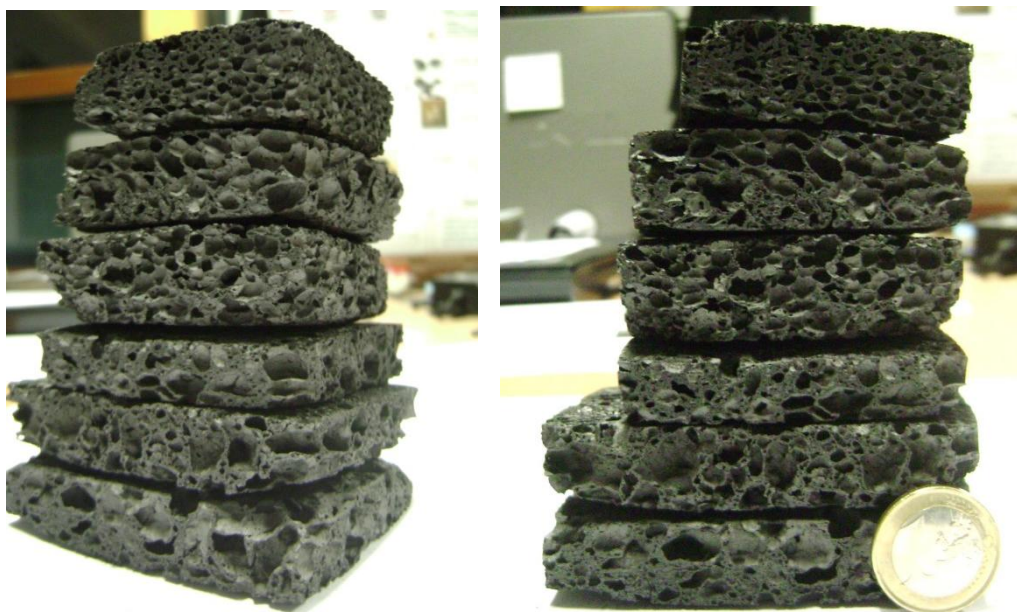


Fig. 1. Typical composite (sucrose char / graphite particles) carbon foams for seasonal STES based on sugar alcohols. Each sample is about 1.5 cm thick and 6 – 7 cm long, on average.

2.2 Hydrophobisation of carbon foams

Various kinds of surface treatment were considered here for making sucrose-based carbon foams more hydrophobic: direct fluorination with molecular fluorine, silanisation, chemical grafting of perfluoroalkyl chains, and electrochemical grafting of fluorinated moieties.

2.2.1 *Direct fluorination by molecular F_2*

Direct fluorination by F_2 is the easiest method for covalent grafting of fluorine atoms onto carbon materials and guarantees a very homogeneous treatment when the treatment conditions are optimised. However, because the present materials were composite foams, i.e., containing two kinds of carbon (sucrose char and graphite) with very different reactivities, many trials had to be carried out to find the best way of fluorinating them. All the corresponding details are given in section I of the Supplementary Information, leading to Figs. S1 – S6. A lot of information about the reactivity of carbon with fluorine is also given there, supporting the

need of multiple preliminary trials for getting a material of relevant composition for the intended application.

2.2.2 Silanisation

Sucrose-based composite carbon foams were covered by silica using a sol-gel process described elsewhere and already successfully carried out for hydrophobising activated carbons [30] and, more recently, organic foams for thermal insulation [31]. In order to promote the grafting of silane, the carbon surface was first oxidised to create as much surface functions as possible. Then, decarboxylation was carried out by heating the material, and the remaining oxygenated surface functions were selectively reduced into hydroxyls. Finally, vinyltrimethoxysilane (vtmos) was grafted by refluxing in dry toluene. The scheme of the process is given in Fig. S7, and the equipment used for the last step is shown in Fig. S8 of the Supplementary Information. The resultant sample was named CF900_vtmos.

2.2.3 Grafting of perfluoroalkyl chains

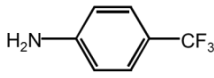
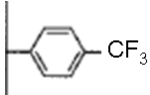
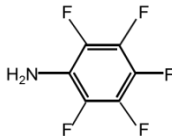
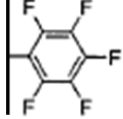
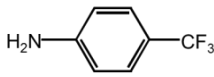
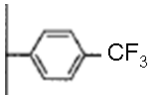
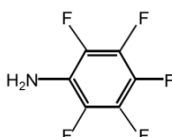
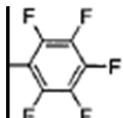
Grafting long perfluoroalkyl chains was carried out in a very similar way as before, using a method inspired from [32]. Composite carbon foam (1.82 g) was again first oxidised in nitric acid, washed, then heat-treated at 450°C in N₂ atmosphere, and reduced by NaBH₄ (0.5 g in 100 mL of dry ethanol). Then, the resultant carbon foam was soaked in 100 g of methanol containing 1 g of perfluorodecyltrimethoxysilane (pfdtms). The resultant mixture was stirred (300 rpm) for 3 h (see Fig. S9 of the Electronic Supplementary Information). The grafted sample was finally thermally treated at 140°C in N₂ atmosphere, and was called CF900_pfdtms.

2.2.4 Electrochemical grafting of fluorinated moieties

Since carbon is an electrically conducting material, grafting fluorinated functions has been possible by electrochemical reduction of diazonium salts according to a procedure described elsewhere [33]. All experimental details are given in the Supplementary Information, especially the general scheme of the process in Fig. S11. The experimental device and typical voltammograms are shown in Fig. S12.

Four samples of grafted carbon foam were first prepared, in aqueous sulphuric acid (0.1 mol L⁻¹) or in acetonitrile containing NBu₄BF₄ (0.1 mol L⁻¹) as electrolyte, and from two amines as diazonium precursors: trifluoro-methyl-aniline and pentafluoro-aniline, leading to the functionalisation of carbon surface by -C₆H₅CF₃ and -C₆F₅ groups, respectively. The preparation conditions are summarised in Table 1.

Table 1. Conditions of electrochemical reduction of diazonium salts for grafting aromatic fluorinated moieties (amine concentration 2×10^{-3} mol L⁻¹, tBuNO₂ or NaNO₂ 6×10^{-3} mol L⁻¹).

Sample name	Solvent used	Initial amines	Grafted function
H ₂ SO ₄ -CF ₃	Aqueous H ₂ SO ₄ (0.1 mol L ⁻¹)		
H ₂ SO ₄ -CF ₅	Aqueous H ₂ SO ₄ (0.1 mol L ⁻¹)		
ACN-CF ₃	Anhydrous CH ₃ CN (NBu ₄ BF ₄ 0.1 mol L ⁻¹)		
ACN-CF ₅	Anhydrous CH ₃ CN (NBu ₄ BF ₄ 0.1 mol L ⁻¹)		

2.3 Infiltration of carbon foams with molten sugar alcohols

A eutectic xylitol-erythritol blend, prepared by mixing 64 parts of xylitol and 36 parts of erythritol, was used. In the following, such intimate blend will be referred to as Molecular Alloy based on Sugar Alcohols (MASA). The physical properties of xylitol, erythritol and MASA are shown in Table 2.

Given the hydrophobic nature of studied carbon foams, vacuum-assisted infiltration is necessary to prepare the carbon foam – sugar alcohol composites. It is well known that a porous medium with interconnected (open) porosity can be infiltrated with a non-wetting fluid by establishing a pressure difference between the inside and the outside (ΔP), which forces the intrusion of fluid into the porous structure. The minimum ΔP required for intrusion to occur is determined by the Young-Laplace equation [34]: $\Delta P = -\sigma \cos\theta / (kr)$, where σ and θ are, respectively, the surface tension and the contact angle. r is the pore diameter and k is the geometry coefficient of the pores ($k = 1/2$ for cylindrical pores, $k = 1/3$ for spherical pores). The carbon foams studied in this work are characterised by large globular pores of millimetre size [26]. As shown in Table 7, the observed contact angles range from 96° to 155° . The surface tension of sugar alcohols is of the order of 60 mJ/m^2 [35]. Therefore, considering $r = 2 \text{ mm}$, $k = 1/3$, $\theta = 155^\circ$ and $\sigma = 60 \text{ mJ/m}^2$, we obtain $\Delta P = 0.8 \text{ mbar}$, which means that using primary vacuum is largely sufficient to achieve the infiltration of the foam with the molten sugar alcohol.

Sucrose-based carbon – graphite composite foam samples ($5 - 7 \text{ cm}^3$) were first ultrasonically cleaned with water and next dried in a ventilated oven at 120°C for 12 hours. The carbon foams were then impregnated with the xylitol-erythritol (64 / 36 %) blend in a vacuum oven heated at 120°C for 6 hours. After the MASA was molten and infiltrated, the

whole was cooled down to room temperature under vacuum. Under these conditions, it took around 12 hours for the blend to solidify. It should be noted that in DSC experiments, which are rather short, unlike the present case, it is generally not possible to observe the crystallisation of the undercooled eutectic mixture. After solidification, the excess blend was removed from the foam by cutting it with a knife, the carbon-MASA hybrid materials were weighed, and their physical characteristics and properties were measured.

Table 2. Physical properties of sugar alcohols xylitol, erythritol and MASA [25]. The values of density and thermal conductivity are those of the solid phase at room temperature.

Property	Sugar alcohol	Xylitol	Erythritol	MASA
Density (g cm^{-3})		1.52	1.45	1.50 ^(*)
Melting point ($^{\circ}\text{C}$)		92-96	121	82
Latent heat of fusion (J g^{-1})		267	340	270
Thermal conductivity ($\text{W m}^{-1} \text{K}^{-1}$)		1.32	0.76	0.38

^(*) The density of MASA (xylitol-erythritol 64/36 %) was calculated from density data of xylitol and erythritol as $1.52 \times 64/100 + 1.45 \times 36/100 \approx 1.5 \text{ g cm}^{-3}$.

Sucrose-based carbon – graphite composite foam samples infiltrated with molten erythritol were also prepared (called carbon-SA hybrid materials hereafter). They were only used to study the efficacy of hydrophobisation by Differential Scanning Calorimetry (DSC). Although xylitol-erythritol eutectic mixture has more interest for seasonal STES application than erythritol, the latter is preferred for DSC testing because the eutectic presents a very low nucleation rate. This characteristic, which is searched for long-term TES, is however a drawback for DSC testing purpose. On the one hand, it implies too long testing times because of the very long nucleation induction time. On the other hand, it reduces significantly the

sensitivity of subcooling to the chemistry, to the morphology and to the texture of foreign surfaces, which are key parameters that will influence SA nucleation within the studied carbon foams. Therefore, the use of erythritol, which exhibits much faster nucleation kinetics than the xylitol-erythritol mixture, allows both shortening the DSC testing and magnifying the effects of foreign surfaces on nucleation, thus provides a suitable way for evaluating and comparing the different hydrophobisation methods under study.

2.4 Characterisation methods

2.4.1 *Characterisation of carbon foams*

Composite carbon foams were thoroughly characterised in terms of porous structure and surface area, wettability, carbon nanotexture and crystallinity, surface chemistry, thermal conductivity and mechanical properties. All these properties are extremely important for the intended application, since they govern: (i) the ability of the carbon foams to be impregnated in depth by the molten phase-change materials; (ii) the preservation of the sub-cooling; (iii) the level of the thermal transfers; and (iv) the mechanical stability of the whole system. For this purpose, the following analytical methods have been used: adsorption of gases, contact angle measurements, Raman and X-ray photoelectron spectroscopies, nuclear magnetic resonance of ^{19}F , X-ray diffraction, thermal conductivity measurements, and compression tests. All the corresponding details and justification of the experimental choices can be found in section II of the Supplementary Information.

2.4.2 *Calorimetry of SA – and MASA – carbon foam hybrid materials*

Calorimetry tests aimed at evaluating the efficacy of the different hydrophobisation methods in preventing heterogeneous nucleation of the sugar alcohols on the surface of the carbon foams. The carbon-MASA hybrid materials, as well as pure erythritol used as

reference, were tested in two different DSC apparatuses, which are referred to as small-volume DSC (Steraram SENSYS Evo) and large-volume DSC (Setaram MHTC 96) hereafter. The small-volume DSC allows sample volumes up to 0.3 mL to be tested, whereas the maximum volume that is allowed by the large-volume DSC is 6.5 mL. The testing conditions used are detailed in Fig. 2 and Table 3. To minimise the thermal gradients within the samples, especially during the cooling of the subcooled melts, the applied heating/cooling rates were $1^{\circ}\text{C min}^{-1}$ and $0.5^{\circ}\text{C min}^{-1}$ in small and large-volume DSC, respectively. The duration of the isotherm preceding the cooling stage was 15 min in the small-volume DSC but was higher (1 h) in the large-volume DSC to achieve isothermal conditions within the sample before starting the cooling stage. The erythritol content in large samples of hybrid materials varied between 1300 mg and 4470 mg, depending on the sample. Therefore, in order to make comparisons, different samples of pure erythritol were tested within this range of mass. In all cases, the DSC experiments were carried out in open crucibles continuously flushed by high-purity nitrogen. The combination of small- and big-volume-DSC with applied operation conditions thus allowed the effect of key external parameters on subcooling, such as sample volume and cooling rate, to be studied.

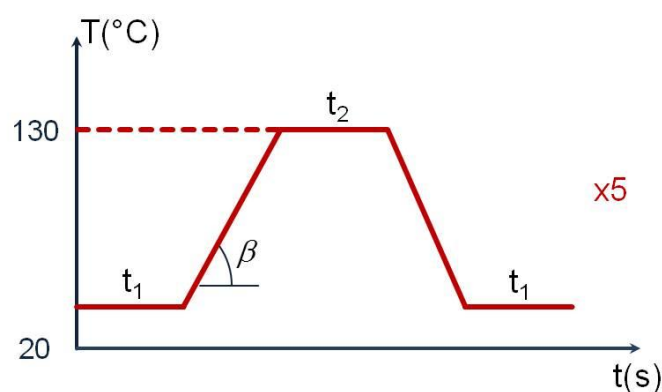


Fig. 2. Temperature cycle used in DSC experiments, see also Table 3 for details.

The same DSC tests were used to analyse whether or not the confinement of the sugar alcohol into the carbon foam or the applied hydrophobisation treatments modified the melting point or the latent heat of the phase-change material. The melting temperature was determined by the onset temperature of the endothermic peak in the DSC-thermograms, whereas the latent heat was calculated by integration of the latter, assuming a linear baseline. The DSCs were calibrated for heat flow and temperature using high-purity (> 99.99 %) reference materials: indium, tin, zinc and aluminum. The accuracy in the determination of melting temperatures was about ± 1 K, whereas that of the enthalpies of phase transition was ± 5 %.

Table 3. Parameters of the temperature cycle shown in Fig. 2.

	Small volume-DSC	Big volume-DSC
β ($^{\circ}\text{C min}^{-1}$)	1	0.5
t_1 (min)	15	30
t_2 (min)	15	60
Nature of spans	Al	Al
Diameter (mm)	6.17	14
Height (mm)	11.3	45
Mass of erythritol (mg)	ca. 30	1300 - 4770
Total mass (mg)	34 - 37	1750 - 6500

3. Results and discussion

3.1 Characteristics of hydrophobised carbon foams

Structural and thermal properties of the pristine carbon foam were investigated in our former work [26]. Hence, the study now mainly focuses on the analysis of surface chemistry and roughness, which are the main parameters that can influence the wettability properties of the foams and, therefore, the subcooling phenomenon in the encapsulated sugar alcohol. The main features of the different hydrophobised carbon foams are presented in sections 3.1.1 to 3.1.3, whereas wettability properties of all of them are discussed in section 3.1.4.

3.1.1 *Stoichiometry, nanotexture and surface chemistry after direct fluorination*

The compositions of all carbon foams obtained after treatment in pure F₂ in the various dynamic conditions detailed in section I of the Electronic Supplementary Information are given in Table 4. The resultant stoichiometry formula was calculated from the weight uptake of the sample during the fluorination process. As expected, under the same fluorination conditions, the composite (graphite / sucrose char) foams having less reactivity due to their graphite content led to less F-rich compounds than pure sucrose carbon foams [36]. Besides, the fluorination increased for all the foams when increasing the temperature of the F₂ stream. The nanotexture of these materials has been investigated by Raman spectroscopy, ¹⁹F NMR was used to study the surface chemistry, and XRD was employed to analyse whether direct fluorination may have modified the carbon structure. Nitrogen and carbon dioxide adsorption studies were not carried out on these materials because of the risk of desorbing highly corrosive fluorine compounds during the degassing step.

Table 4. Stoichiometry of fluorinated carbons obtained by direct fluorination with F₂ under dynamic conditions.

Samples	Dynamic F ₂ (1 h, 300°C)	Dynamic F ₂ (1 h, 280°C)	Dynamic F ₂ (1 h, 180°C)
Pure sucrose-based carbon foam		CF _{0.23}	CF _{0.09}
Graphite / sucrose char composite carbon foam	CF _{0.21}	CF _{0.07}	CF _{0.02}

The Raman spectra of pure sucrose-based carbon foams and composite (graphite/sucrose char) foams are shown in Fig. 3. Pure sucrose-based carbon foam has, as expected, a rather disordered carbon structure since the intensity of the G band is only slightly higher than that of the D-band. Fluorination in increasingly harsh conditions did not really change this characteristic, suggesting that the additional disorder that has been introduced by the chemical treatment is negligible. Fluorine indeed first reacts with the more reactive carbon areas, i.e., with the most disordered ones (edges of carbon layers and other structural defects), reducing their extent and letting the most organised parts of the material almost unchanged, at least at the beginning of the reaction. However, a shift of D- and G-bands towards lower wavenumbers can be seen when the severity of the fluorination increased, and corresponds to an increasing number of sp³ carbons. The D-band is thus shifted towards the expected position of diamond. Furthermore, it is known that the D-band shift is correlated linearly to the F/C atomic ratio of the compound [37].

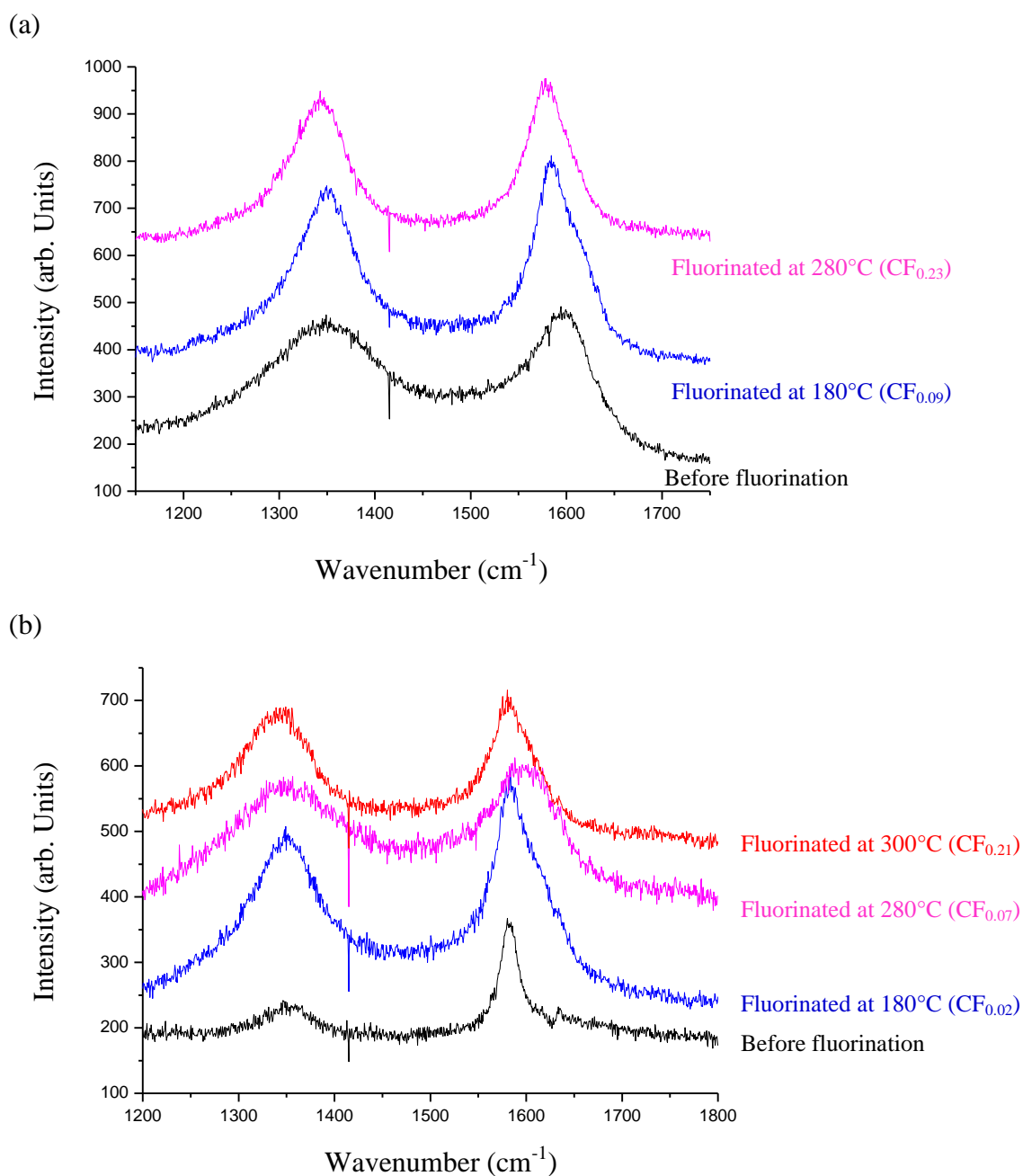


Fig. 3. Raman spectra of carbon foams before and after direct fluorination in a stream of hot molecular F_2 at different temperatures indicated on the plots: (a) pure sucrose-based carbon foam; (b) composite carbon foam.

Carbon composite foam before fluorination presents a much more intense G-band, attributed to the graphite particles it contains. After fluorination, the G/D intensity ratio decreased when the treatment temperature increased, thus evidencing the disorder in the

carbon structure induced by fluorination. At the highest temperature, the G/D intensity ratio was very similar to that of the pure, non-treated, sucrose-based carbon foam. The same shift of the D-band was observed, having the same meaning as before, i.e., an increase of the F content.

^{19}F NMR spectra are shown in Fig. 4. Despite the high Magic Angle Spinning speed (34 kHz), superimposition of spinning sidebands (marked by asterisks) and isotropic bands could not be completely avoided. The main band at a chemical shift in the -160 – -190 ppm range is assigned to the covalent C-F bonds [37-43]. Because this band consists in the superimposition of components related to different covalent C-F bonds, more or less weakened by hyperconjugation (see section I of the Supplementary Information for details), the narrower is this band, the more homogeneous is the chemical environment, i.e., the lower is the number of different fluorinated species close to the considered C-F bond. This is what happens in a carbon foam destroyed at composition $\text{CF}_{\sim 1}$ and with fluorinated graphite obtained under static fluorination conditions at 450°C.

Regarding the materials fluorinated in dynamic conditions (Table 4, Fig. 4), the following comments can be made. The chemical shift of the C-F bonds clearly increases when composite and pure carbon foams of low F content (with respect to highly fluorinated graphite and foam) are considered. It is indeed well known that the chemical shift moves toward higher positive values when the covalence of the C-F bond decreases. Indeed, hyperconjugation involving C-C bonds into the carbon sheets and C-F bonds results in the lowering of the C-F bonding order, from covalent to semi-covalent and semi-ionic [38,44]. Such hyperconjugation is allowed by the coexistence of conjugated C-C double bonds into non-fluorinated parts and covalent C-F bonds in corrugated fluorocarbon regions.

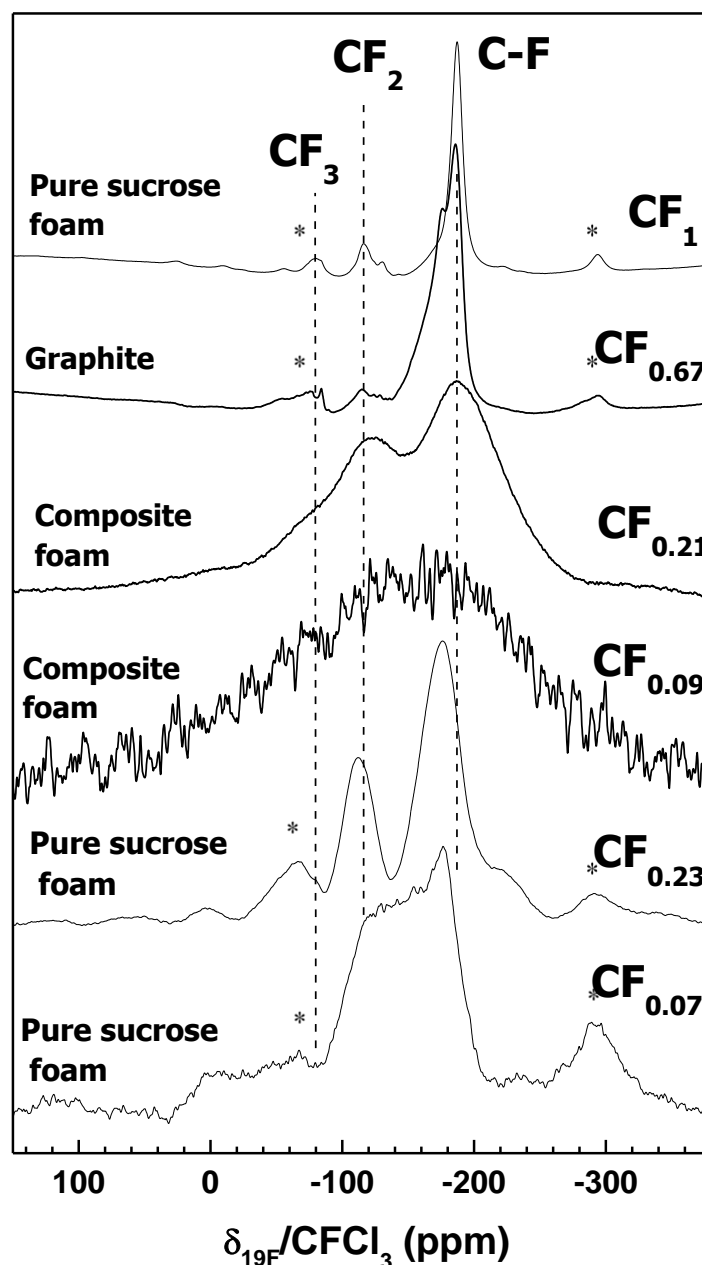


Fig. 4. MAS ^{19}F NMR spectra (30 kHz) of several carbon materials submitted to direct fluorination in a stream of hot F_2 . The asterisks just mark spinning bands.

The low amount of F in the formula of fluorinated composite foams, and the temperatures which have been used for preparing $\text{CF}_{0.09}$, suggest that the graphite did not react with F_2 and remained electrically conducting in the absence of sp^3 carbons. The presence of free electrons disturbed the acquisition of the NMR signal, hence the very noisy spectra of $\text{CF}_{0.09}$ despite

similar recording conditions (scan number and received gain). This obviously does not apply to $\text{CF}_{0.21}$.

Rather high amounts of CF_2 groups are evidenced in fluorinated, pure sucrose-based, carbon foam. These F-rich moieties originate from the reaction of carbon layers edges and structural defects, initially present in higher amounts. Higher reaction temperature made the number of CF_2 and CF_3 groups increase, the next step being the burning of the foam into CF_4 and C_2F_6 . Finally, the spectra of $\text{CF}_{0.07}$ is noisier than that of $\text{CF}_{0.23}$ only because of the lower amount of F, which decreased the signal/noise ratio.

As the covalent grafting of fluorine atoms by F_2 has been proved by ^{19}F NMR, XPS was not performed with these samples.

XRD studies have been carried out to see whether direct fluorination may have modified the carbon structure. The corresponding XRD patterns are given in Fig. 5, where the effect of grafting fluorinated functions is also shown for comparison. The intense, narrow bands in the pristine composite carbon foams correspond to the graphite filler, whereas the diffusion background is mainly due to the highly disordered sucrose-based carbon. The comparison with the fluorinated material suggests that the chemical treatment was mostly superficial, since no significant change could be noticed. As shown in the Electronic Supplementary Information (Fig. S13), modelling the XRD pattern at Bragg angles ranging from 40 to 50° indicates that the fraction of rhombohedral phase of graphite in the composite carbon foam after fluorination by molecular F_2 (7.2 %) is decreased compared to that found for non-treated composite foam (9.7 %). The higher reactivity of rhombohedral graphite compared to hexagonal graphite explains that the volume fraction of the former decreased upon fluorination. Fig. 5 also evidenced that grafting perfluorodecyltrimethoxysilane did not change anything to the bulk of the carbon structure, as expected. Since grafting

vinyltrimethoxilane also is a surface modification only, no additional XRD study was carried out.

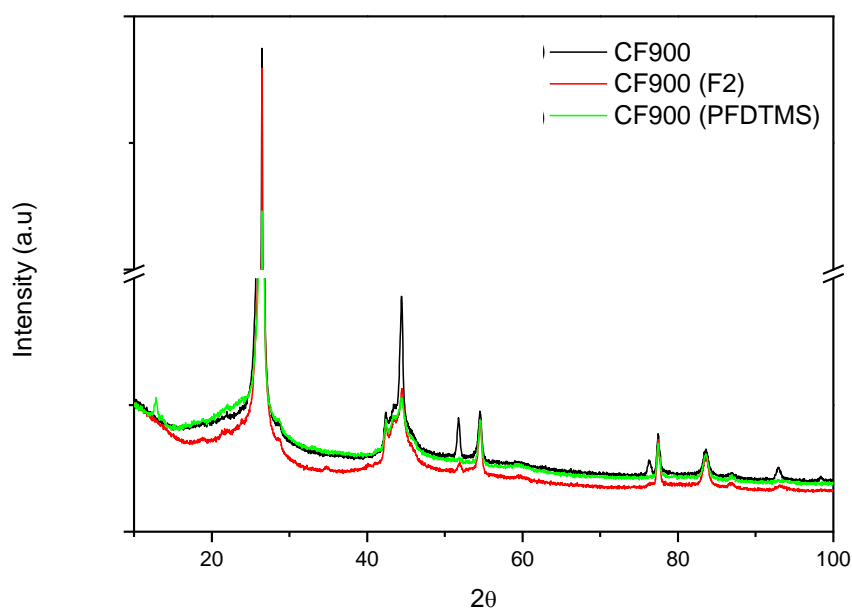


Fig. 5. XRD patterns of composite carbon foam before fluorination (CF900) and after fluorination by molecular F_2 (280°C, 1h: $CF_{0.07}$) or by chemical grafting of perfluorodecyltrimethoxysilane (pfdtms, heated at 140°C).

3.1.2 Porous texture after silanisation and grafting of perfluoroalkyl chains

Nitrogen adsorption-desorption isotherms of the composite carbon foam before chemical grafting, referred to as CF900, are shown in Fig. 6(a), and the corresponding carbon dioxide adsorption isotherm is given in Fig. 6(b). Those of samples grafted with vtmos and with pfdtms are also presented in Fig. 6.

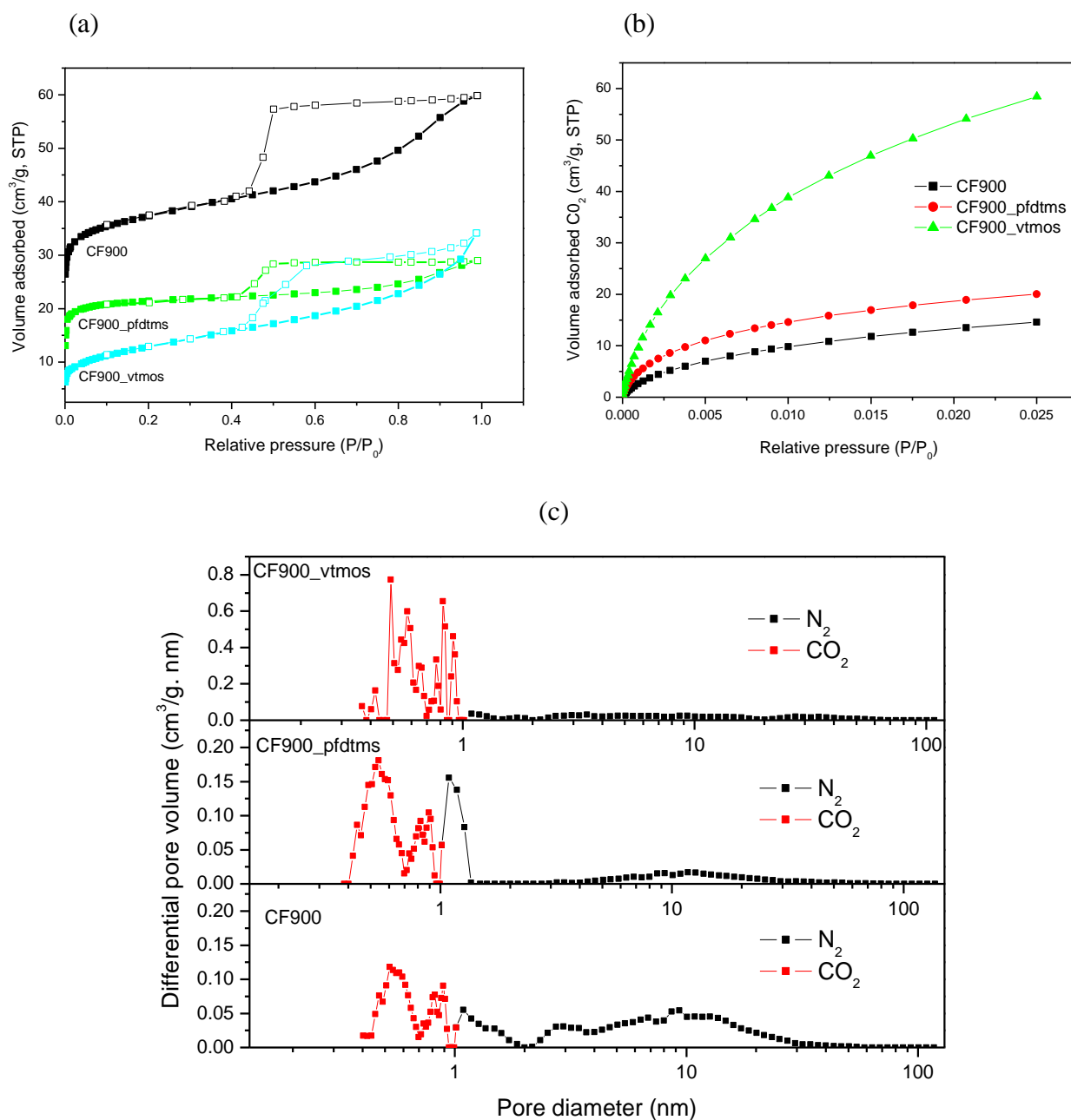


Fig. 6: Adsorption isotherms of composite carbon foam before and after surface treatment by chemical grafting of silica (through vtms) and pfdtms (heated at 140°C): (a) Nitrogen (full and empty symbols stand for adsorption and desorption, respectively), and (b) carbon dioxide, used as molecular probes. (c) Corresponding pore size distributions of composite carbon foams before (CF900) and after surface treatment by chemical grafting of silica (through vtms) and of pfdtms, using nitrogen and carbon dioxide as molecular probes.

All N₂ isotherms are combinations of types I and IV, according to the IUPAC classification [45], characteristic of micro-mesoporous materials. The adsorbed amounts are low, which indicates that the corresponding pore volumes are also low, unlike the macroporosity that can never be evidenced by adsorption techniques. Surface treatments led to lower adsorbed volumes with respect to the reference sample CF900 with a corresponding decrease of the plateau height, which indicates that a significant amount of microporosity (pores < 2 nm) has been lost. CO₂ isotherms evidenced the opposite trend, i.e., an increase of microporosity induced by surface treatment. The corresponding data are given in Table 5. Based on the value of surface area, the amounts of reactants required for the chemical grafting of vtmos and pfdtms could be calculated as explained in the Supplementary Information.

Table 5. Pore texture parameters derived from Fig. 6.

Sample	A_{BET} (m ² g ⁻¹)	$V_{0.99}$ (cm ³ g ⁻¹)	V_{μ} (N ₂) (cm ³ g ⁻¹)	V_{μ} (CO ₂) (cm ³ g ⁻¹)	V_m (cm ³ g ⁻¹)
Non-treated composite foam	140	0.093	0.054	0.050	0.04
Treated with pfdtms (140°C)	84	0.045	0.038	0.063	0.01
Treated with vtmos	46	0.053	0.017	0.208	0.04

A_{BET} : apparent surface area; V_{μ} : micropore volume; $V_{0.99}$: total pore volume; V_m : mesopore volume. See section II of the Supplementary Information for details of their calculation.

It is useful to recall here that CO₂ allows probing narrower pores than N₂. Thus, finding almost similar values of V_{μ} (CO₂) and V_{μ} (N₂) for the non-treated carbon foam indicates that no extremely narrow micropores exist in this material. In contrast, the chemical treatment blocked the wider micropores, but created new narrow micropores inside the grafted layer.

In N₂ isotherms, all the hysteresis cycles at high relative pressure are broad and of H2 type. Type H2 corresponds to porous channels with a pore mouth smaller than the pore body (this is the case of ink-bottle-shaped pores). The surface treatments decreased the width of the cycles, suggesting a slight loss of mesoporosity (2 nm < pores < 50 nm), see again Table 5.

The pore size distributions calculated by application of Density Functional Theory (DFT) to the isotherms are presented in Fig. 6(c). They clearly confirm the decrease of the amount of wide micropores (black curves) and the increase of the amount of narrow micropores (red curves) after surface treatment. As expected, CO₂ allowed to complete and to extend the pore size distribution in the narrow pore range of the plot.

3.1.3 *Surface chemistry after electrochemical grafting of fluorinated moieties*

X-ray photoelectron spectroscopy (XPS) studies were performed on samples treated by electrochemical diazonium salt reduction, thanks to which the surface composition could be estimated. Representative examples of the corresponding spectra are given in Fig. S14 of the Supplementary Information, and the results for all samples are reported in Table 6. As the covalent grafting of fluorine atoms by F₂ has been proved by ¹⁹F NMR, XPS was not performed with those samples.

The quantification of the amount of fluorine at the surface is given by the at.% of F from the C1s bands. The amount of F in C-F bonds only is given by the at.% of F from the F1s band. The difference between C1s and F1s thus corresponds to the at.% of F involved in CF₂ and CF₃ groups. The sample H₂SO₄-CF₅, i.e., prepared in 0.1 mol L⁻¹ H₂SO₄ with pentafluoro-aniline, presents 19.75 at.% of F at its surface. The fluorine content is thus the highest in this material, followed by ACN-CF₃ (8.29 at.%), H₂SO₄-CF₃ (6.70 at.%) and ACN-CF₅ (1.13 at.%) for which the grafting was poor. But electrochemical grafting in H₂SO₄

also induced an increase of oxygen at the surface, and the O content of H₂SO₄-CF₅ was also the highest (9.9 at.%). Therefore, it is possible that the positive effect of –C₆F₅ groups with respect to hydrophobisation can be reduced by an enhanced hydrophilicity due to a higher number of oxygenated moieties. These results also show the significant impact of the grafting conditions, since a same molecule (see again Table 1) can produce very different fluorine concentrations at the carbon surface. This is especially the case with pentafluoro-aniline, which produced the highest atomic F fraction when grafted in H₂SO₄, but the lowest one in acetonitrile.

Table 6. XPS results in terms of binding energy (BE, expressed in eV) of elements C (C1s of CF, CF₂ and CF₃ groups), F (F1s of CF bonds) and O (O1s), and corresponding abundance (expressed in atomic %).

	C1s bands		F1s bands		O1s	
	BE (eV)	at. %	BE (eV)	at. %	BE (eV)	at. %
Non-treated foam						2.72
H ₂ SO ₄ -CF ₃	286 – 293	6.70	686 – 689	5.10	532 – 534	4.02
H ₂ SO ₄ -CF ₅	286 – 293	19.75	686 – 689	15.28	532 – 534	9.90
ACN-CF ₃	286 – 293	8.29	686 – 689	6.87	532 – 534	3.13
ACN-CF ₅	286 – 293	1.13	686 – 689	0.38	532 – 534	3.56

The samples hydrophobised by electro-reduction of diazonium salts were not investigated by adsorption methods, neither by XRD. On the one hand, the amount of material produced is too low for getting a meaningful information of their porous texture by absorption methods.

On the other hand, electrochemical grafting involves a surface modification only (such as grafting perfluorodecyltrimethoxysilane above) and, therefore, it is not expected that it changes anything to the bulk of the carbon structure.

3.1.4 Wettability properties

The water contact angles, obtained by fitting the (circular) shape of the water droplet deposited on the surfaces of the carbon foams, themselves fitted by a linear baseline, are presented in Table 7. The values show that, whatever the treatment, an increase of contact angle is observed. Whereas the non-treated foam was already spontaneously (although moderately) hydrophobic, an enhanced hydrophobicity was noticed, but the effects are very different from each other. The highest hydrophobic character was obtained by direct fluorination at the highest amount of F incorporated in the carbon structure ($CF_{0.07}$), but the chemical grafting of perfluoroalkyl chains (pfdtmos) also had a significant effect. Silanisation by vtmos also proved to be as effective as the latter treatment. In comparison, the electrochemical grafting of fluorinated surface groups was rather disappointing and, unexpectedly, some treatments of this kind ($H_2SO_4-CF_3$, $ACN-CF_3$, $ACN-CF_5$) were even almost ineffective with respect to the raw carbon foam.

Overall, the values presented in Table 7 are in good agreement with former data reported in the literature. The presence of fluorine atoms on the carbonaceous surface through covalent C-F bonds indeed allows an increase of the hydrophobic character of, for instance, carbon fibers [46,47], even at low fluorine content for which the advancing water contact angle increases up to 115° (102° for $CF_{0.02}$ composition) [48]. In comparison, flat polytetrafluoroethylene (PTFE) exhibits a contact angle of 110° . The grafting of pfdtmos on organic foams has been shown to lead to contact angles ranging from 137 to 143° [31], whereas the same applied to ordered mesoporous carbons gave 150° [49]. As for the

deposition of silica, a rather broad range of contact angles has been reported, typically from less than 60° to 120° [50], and even up to 165° [51] due to different final surface roughness.

Table 7. Contact angles measured for non-treated and hydrophobised carbon foams.

Hydrophobisation treatment	Contact angle (°)
None	96.1 ± 4.3
vtmos	133.9 ± 2.5°
pfdtmos	128.7 ± 4.5°
F ₂ (280°C, 1 h): CF _{0.07}	155.2 ± 1.4°
F ₂ (180°C, 1 h): CF _{0.02}	123.1 ± 3.8°
H ₂ SO ₄ -CF ₃	99.2 ± 2.7°
H ₂ SO ₄ -CF ₅	110.9 ± 3.1°
ACN-CF ₃	101.8 ± 3.0°
ACN-CF ₅	98.0 ± 1.5°

Indeed, surface roughness and possible nano/micro-texturation can account for improved hydrophobicity. Only the Cassie-Baxter equation [52], contrary to Wenzel's one [53], can predict extremely high contact angles, which indicate the presence of air between the droplet and the surface. The Cassie-Baxter equation can be written as $\cos \theta = r_f f \cos \theta_s + f - 1$, where θ_s is the contact angle measured on a smooth surface, r_f is the roughness ratio of the substrate wetted by the liquid, f the solid fraction and thus $(1 - f)$ is the fraction of air. This equation can lead to superhydrophobic properties if the air fraction is extremely high and to very (yet not “super”) hydrophobic properties if the air fraction is less important. Many examples of this effect have been reported in the literature. The combination of surface chemistry and local roughness of carbon foams surfaces thus explains the range of values observed in Table 7.

3.2 Properties of MASA – carbon foam hybrid materials

3.2.1 Impregnation by MASA

Two samples of non-treated composite carbon foam, whose characteristics are listed in Table 8, were tested for calculating the yield of impregnation by a molten blend of xylitol and erythritol. After impregnation, their characteristics changed according to the values presented in the same Table 8. It can be seen from the latter that 85 – 86% of the total porosity of the carbon foams has been filled. Pictures of sample #1 before and after impregnation are shown in Fig. 7. A second impregnation carried out in the same conditions only increased the yield up to 91%. Of course, the resultant hybrid materials cannot retain the PCM by capillary action once it has melted within the porous support structure. Indeed, due to the hydrophobic characteristics of the carbon foams, spontaneous extrusion of the liquid from the pores may occur. From a practical point of view, this means that the proposed hybrid materials must be properly enclosed in the storage vessel to prevent leakage.

Table 8. Main characteristics of composite carbon foams before and after impregnation.

Impregnation	Sample #	Mass (g)	Volume (cm ³)	Density (g cm ⁻³)	Porosity (%)	Initial pore volume (cm ³)	Infiltrated MASA volume (cm ³) ^a	Infiltration yield (%) ^b	Thermal conductivity (W m ⁻¹ K ⁻¹)
Before	1	8.13	25.4	0.32	85.8	21.79	-	-	3.1
	2	7.92	24.7	0.32	85.8	21.19	-	-	3.1
After	1	36.5	25.4	1.44	-	21.79	18.91	86.8	3.6
	2	34.8	24.7	1.41	-	21.19	17.92	84.6	3.6

^a assuming a blend density of 1.5 g cm⁻³

^b defined as the ratio: Infiltrated MASA volume (cm³) / Initial pore volume (cm³)

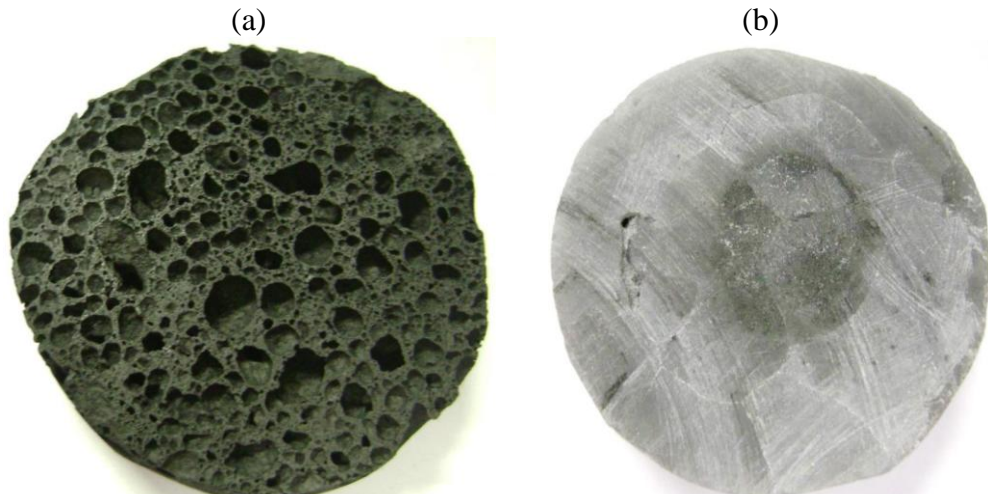


Fig. 7: Photographs of composite carbon foam: (a) before MASA impregnation; (b) after one single MASA impregnation. The diameter of the sample is close to 6 cm.

XRD studies were then carried out for detecting whether the presence of the carbon foam surface modified or not the structure of the solidified xylitol – erythritol (64 /36 %) blend after infiltration in the porous structure. Fig. 8(a) gathers the XRD patterns of: (i) composite carbon foam alone (CF900 in this plot); (ii) MASA blend alone; and (iii) MASA-carbon foam hybrid material. It can be seen that the peaks of the latter are exactly the same as those of the MASA alone, and also perfectly overlap those of the porous carbon in which the blend was infiltrated. It can therefore be concluded that no change of crystalline structure, possibly induced by the confinement in the porous carbon structure, happened.

Two samples of two kinds of hydrophobised carbon composite foams were tested for measuring the impregnation yield by the MASA: (i) grafted with pfdtms; and (ii) directly fluorinated with F_2 at $280^\circ C$ during 1 hour. The corresponding characteristics of these materials before impregnation are listed in Table 9.

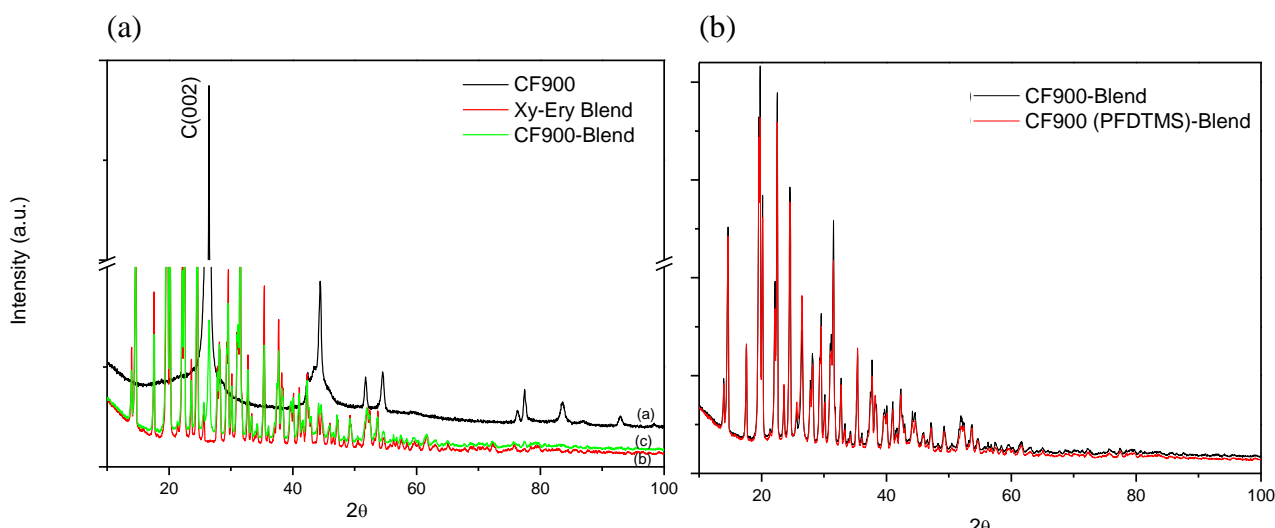


Fig. 8. XRD patterns of (a) CF900 alone (black), xylitol-erythritol blend alone (red) and CF900 impregnated with xylitol-erythritol blend (green); and (b) CF900 impregnated with xylitol-erythritol blend before (black) and after (red) hydrophobisation by pfdtms.

The impregnation protocol carried out in the same conditions as for the non-treated carbon foams (same xylitol – erythritol blend, same temperature, same impregnation time, same vacuum oven) led to the following observation. Unlike what happened with pristine carbon foams, the MASA did not solidify and the foam floated at the surface of the liquid blend. It was necessary to push the foam beneath the surface of the molten blend and to keep the material at 120°C for 6 additional hours before cooling down to room temperature. But the blend took around 24 hours to solidify. After solidification, the excess blend was removed with a knife from the carbon-MASA composite materials, which could be investigated. Their new characteristics are given in the second part of Table 9.

The second part of Table 9 shows that the efficiency of the impregnation dramatically decreased with respect to non-hydrophobised foams, since the impregnation yield was significantly lower than what was found for non-treated samples. Only 54 – 72 % of the total porosity was indeed filled. Hydrophobisation, although not changing the macroscopic

porosity, made the vacuum impregnation much less efficient. For samples treated with pfdtms, a second impregnation was thus tried in the same conditions as for the first one. The results are also given in Table 9. They show that the impregnation ratio increased significantly, but remained lower than typical values of non-hydrophobised foams.

Table 9. Main characteristics of hydrophobised carbon foam samples before and after MASA impregnation.

Before MASA impregnation							
Hydrophobisation method	Sample #	Stoichiometry	Mass (g)	Volume (cm ³)	Density (g cm ⁻³)	Porosity (%)	Thermal conductivity (W m ⁻¹ K ⁻¹)
pfdtms	1	-	1.82	5.7	0.32	85.8	3.1
pfdtms	2	-	1.80	5.6	0.32	85.8	3.1
F ₂	1	CF _{0.03}	2.02	6.3	0.32	85.8	3.2
F ₂	2	CF _{0.05}	1.89	5.9	0.32	85.8	3.2
After MASA impregnation							
Hydrophobisation method	Sample #	Mass (g)	Density (g cm ⁻³)	Initial pore volume (cm ³)	Infiltrated blend volume (cm ³)	Infiltration yield (%)	Thermal conductivity (W m ⁻¹ K ⁻¹)
pfdtms	1a	6.34	1.11	4.89	3.09	63.2	3.3
pfdtms	2a	6.88	1.23	4.80	3.45	71.9	3.3
pfdtms	1b	7.4	1.30	4.89	3.80	77.7	3.3
pfdtms	2b	7.6	1.36	4.80	3.93	81.9	3.3
F ₂	1	6.43	1.02	5.41	2.94	54.3	3.2
F ₂	2	6.25	1.06	5.06	2.91	57.5	3.2

NOTE: Samples pfdtms 1a and 2a correspond to one MASA impregnation, whereas samples pfdtms 1b and 2b refer to previous ones after a second MASA impregnation.

Just like before, XRD studies have been carried out to check any possible effect of the hydrophobised carbon surface towards the crystallisation of the xylitol – erythritol blend. Fig. 8(b) compares the XRD patterns of the MASA-carbon foam hybrid materials: (i) based on pristine composite carbon foam, and (ii) based on composite carbon foam hydrophobised by pfdtms. It can be seen that the two patterns are again identical, and that the peaks are also the same as those of the pure xylitol – erythritol blend. It can therefore be concluded that no change of crystalline structure, possibly induced by the hydrophobisation of the porous carbon structure, happened.

3.2.2 Thermal and mechanical properties

The impact of the surface treatment on the thermal conductivity of the composite carbon foam designed to serve as porous host for enhancing the thermal transfer towards phase-change materials was checked. The conductivity of the pristine composite carbon foams was indeed $3.1 \text{ W m}^{-1} \text{ K}^{-1}$ (see again Table 8) [26], and this value should ideally not decrease due to some possible thermal resistance created by the surface treatment. Whatever the kind of hydrophobisation, no change of thermal conductivity outside of the typical uncertainty for this kind of measurement could ever be observed, as expected from so thin and superficial chemical modification. For instance, as seen in Table 9, the samples hydrophobised by pfdtms and by molecular F_2 have thermal conductivities of 3.1 and $3.2 \text{ W m}^{-1} \text{ K}^{-1}$, respectively. The treated carbon foams can therefore be considered as hydrophobised without any drawback with respect to their initial requirements, i.e., as high porosity and as high thermal conductivity as possible at the same time.

In contrast, replacing the air filling the porosity of the carbon foams by solid MASA was expected to have a significant impact. Thermal conductivity studies of the blend alone and of the blend-carbon foam hybrid materials were then carried out at room temperature. The

measured thermal conductivity of the solid MASA alone was found to be $0.65 \text{ W m}^{-1} \text{ K}^{-1}$. After impregnation, the thermal conductivity of the MASA-carbon foam hybrid materials reached $3.6 \text{ W m}^{-1} \text{ K}^{-1}$ (see again Table 8).

Such 16% increase with respect to the non-impregnated composite carbon foam is readily explained by the higher thermal conductivity of the MASA compared to that of air ($0.0257 \text{ W m}^{-1} \text{ K}^{-1}$) at room temperature. Indeed, the thermal conductivity of open-cell foams, κ ($\text{W m}^{-1} \text{ K}^{-1}$), is expected to follow the well-known equation of Gibson and Ashby [54], which reads (neglecting the contribution of radiative transfer, quite low at room temperature):

$$\kappa = \Phi \kappa_g + \frac{1}{3} \kappa_s (1 - \Phi) \quad (1)$$

where Φ (dimensionless) is the porosity, κ_s ($\text{W m}^{-1} \text{ K}^{-1}$) is the solid thermal conductivity (i.e., the thermal conductivity excluding the sample porosity), and κ_g ($\text{W m}^{-1} \text{ K}^{-1}$) is the thermal conductivity of the gas saturating the porosity. In our former work, κ_s was found to be $65 \text{ W m}^{-1} \text{ K}^{-1}$ [26]. Filling the porosity of the foam with a MASA having a thermal conductivity κ_{MASA} ($\text{W m}^{-1} \text{ K}^{-1}$) and with an infiltration yield Y (dimensionless) leads to Eq. (2):

$$\kappa = Y \Phi \kappa_{MASA} + (1 - Y) \Phi \kappa_g + \frac{1}{3} \kappa_s (1 - \Phi) \quad (2)$$

Using the average infiltration yield $Y = 0.85$ taken from Table 8 and the measured value $\kappa_{MASA} = 0.65 \text{ W m}^{-1} \text{ K}^{-1}$, one finds that the thermal conductivity of the MASA – carbon foam hybrid material is $3.55 \text{ W m}^{-1} \text{ K}^{-1}$, in excellent agreement with the measurements. This is a very positive finding for the foreseen (seasonal STES) application that the thermal conductivity of MASA-carbon foams hybrid materials is always higher than that of each individual component.

After hydrophobisation, and as already shown in the second part of Table 9, the yield of the first infiltration was lower than without surface treatment. Consequently, the hybrid materials based on hydrophobised foams after a first MASA impregnation had a slightly lower thermal conductivity than that of materials prepared from non-treated carbon foam. After a second impregnation, however, the thermal conductivity of samples hydrophobised by pfdtms did not change and remained equal to $3.3 \text{ W m}^{-1} \text{ K}^{-1}$. All these values are lower than what can be calculated from Eq. (2) using the data of infiltration yields given in Table 9. In contrast, Eq. (2) led to excellent predictions when non-treated carbon foams were used. This finding suggests that a non-negligible thermal resistance exists between the hydrophobised surface of carbon foam and the MASA, which might favour undercooling, and which is the desired effect once the MASA has been molten for storing heat. This point will be addressed in the next subsection.

Finally, mechanical tests have been carried out on the hybrid material based on xylitol – erythritol (64 / 36) blend infiltrated in composite carbon foam. Fig. 9 compares the stress–strain compression curves of the composite carbon foam before and after MASA impregnation. The general behaviour did not change after impregnation, since the usual three distinct regions: linear elastic, collapse and densification are observed. The corresponding compressive strengths and elastic moduli calculated from Fig. 9 are listed in Table 10. Impregnation by MASA, which is a hard material after solidification, made the compressive strength and the elastic modulus increase from 3.0 to 9.5 MPa and from 107.5 to 195.9 MPa, respectively.

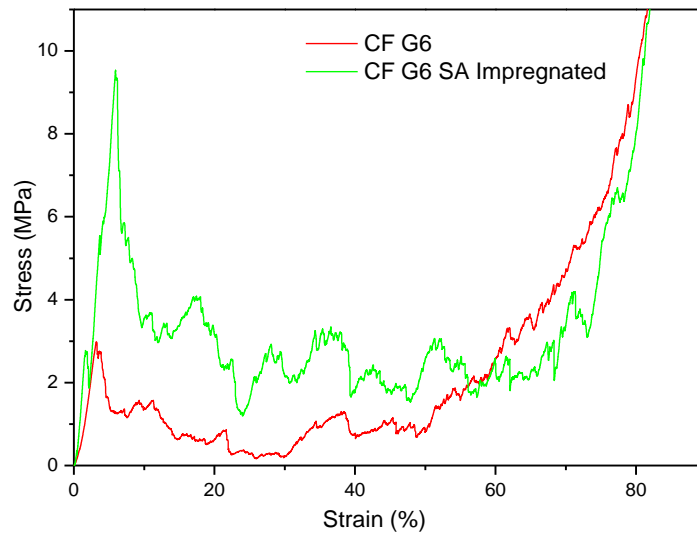


Fig. 9: Stress-strain characteristics of sucrose-based carbon – graphite composite foam before (red) and after impregnation (green).

Table 10: Mechanical properties of composite carbon foam before and after impregnation.

Samples	Compressive strength (MPa)	Elastic modulus (MPa)
Composite carbon foam	3.0	107.5
Impregnated carbon composite foam	9.5	195.9

3.2.3 Effect of hydrophobisation on SA subcooling

The presence of interfaces can modify the nucleation process through various means, such as favourable molecular interactions with the crystallising molecule and a lattice match between the substrate and the compound to be crystallised. In addition, surface morphology, especially in porous structures, is also known to play an important role in controlling nucleation kinetics [55-57].

The heterogeneous nucleation rate, or the number of nuclei surpassing the nucleation barrier per unit area per unit time [58], is a direct measure of the nucleation activity of a

surface with regard to the liquid of interest. Due to the stochastic nature of nucleation events, determining nucleation rates requires statistical measurements performed under exactly the same conditions, involving too long experimental time. However, the objective of this paper was not to perform rigorous analysis of nucleation kinetics but to qualify the ability of hydrophobised carbon foams to prevent heterogeneous nucleation of sugar alcohols and to discard inefficient hydrophobisation methods. To this end, DSC testing as described in section 2.4.2 was used. Indeed, DSC thermograms (temperature vs. compensation heat flux) easily allow identifying the onset of crystallisation and the corresponding temperature. The latter is a good indicator of the SA nucleation activity of a surface, because it can increase dramatically when the presence of this surface lowers the kinetic barriers to nucleation.

Pure erythritol was tested in both small-volume DSC (1 sample of 30.28 mg) and large-volume DSC (3 samples with different masses, see Table 11). In all cases, comparable values for the melting point ($118 \pm 0.5^\circ\text{C}$) and the enthalpy of melting ($340 \pm 17 \text{ J.g}^{-1}$) were obtained. The most relevant information is, however, the temperature of the sample at the onset of the crystallisation (shortly, crystallisation onset). The results achieved are also reported in Table 11, which indicates the crystallisation onset range observed over the five cycles of melting/crystallisation applied, namely $[T_{c,min}, T_{c,max}] \equiv [\min_{k=1 \text{ to } 5} T_{c,k}, \max_{k=1 \text{ to } 5} T_{c,k}]$ where $T_{c,k}$ represents the onset of the crystallisation during the k^{th} cycle. The maximum and minimum subcooling observed, calculated as the difference between the melting temperature and the onset of crystallisation is also given. It can be seen that deep subcooling ($> 68^\circ\text{C}$) is observed in all cases. Moreover, the crystallisation onset range shifts progressively towards higher temperatures as the volume of the sample is increased. This reveals that the nucleation is affected by impurities in the erythritol melt, which act as potential sites for heterogeneous nucleation. It is indeed well

known that, for a fixed value of impurity content in a product, small samples are less likely to contain these foreign agents than large samples, which justifies the increase in subcooling observed with the reduction of sample volume.

Table 11. Results of DSC-testing of pure erythritol and carbon-SA materials with non-hydrophobised foams.

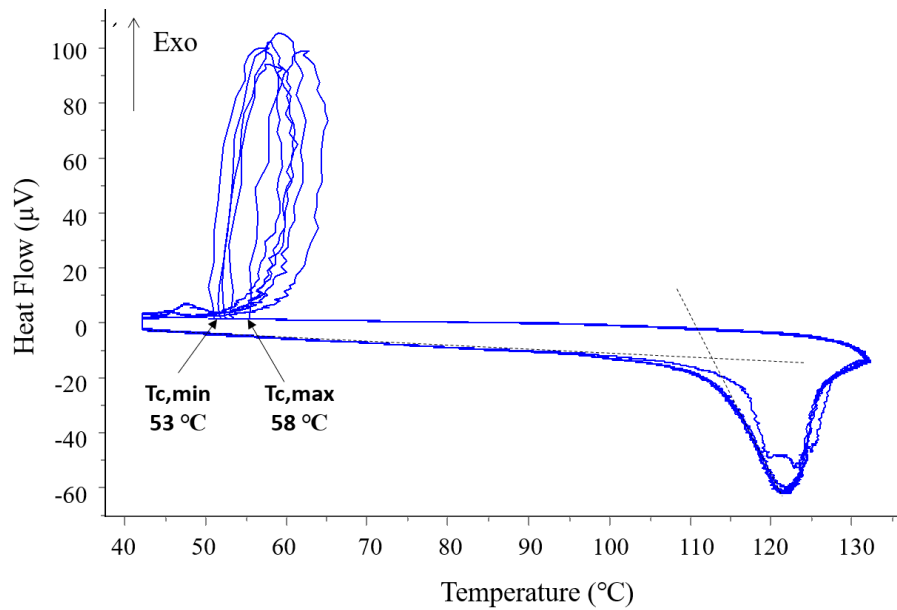
Sample name	Mass of erythritol (mg)	Onset of crystallisation range (°C)	Maximum subcooling observed (°C)	Minimum subcooling observed (°C)
Pure erythritol	4771.73	{46, 50}	72	68
	2707.89	{41, 46}	77	72
	1795.40	{39, 43}	79	75
	30.28	{32, 45}	86	73
CF900 - erythritol	4771.18	{56, 63}	62	55
	1305.53	{53, 58}	65	60
	30.28	{53, 57}	65	61
	29.10	{53, 58.5}	65	59.5

DSC testing for CF900 materials (non-hydrophobised carbon foams) infiltrated with erythritol was also performed for small- and large-volume samples. Fig. 10(a) shows the DSC thermograms (heat flux vs. temperature) obtained for a large-volume sample subjected to five heating and cooling cycles. During heating, all the endothermic (melting) peaks are superimposed except the first one, which, as usual, behaves differently due to thermal resistances of the powders before the first melting. During cooling, the crystallisation of the sample (exothermic peaks) occurs at a much lower temperature than melting. It can be seen that the crystallisation peaks have a loop, which means that the DSC apparatus is not able to dissipate/compensate for the heat flux delivered during sample crystallisation so that the

sample temperature rises. This is typically the case for samples with a high degree of undercooling, where crystallisation is a kind of explosive phenomenon involving a large amount of heat delivered in a very short time that the DSC cannot accommodate. The crystallisation temperature is determined as the onset temperature of the thermal loop (crystallisation peak). It can be seen that, in contrast to melting, the onset of crystallisation is sharp and, therefore, the uncertainty in determining the crystallisation temperature is lower (less than ± 0.5 K approximately) than in melting (± 1 K approximately, according to the calibration performed). The crystallisation onset ranges [$T_{c,min}$, $T_{c,max}$] are reported in Table 11 and are also displayed in Fig. 10(b).

Compared to pure erythritol, it can be seen that: (i) the effect of the volume of the sample is much lower this time (Fig. 10(b)), with comparable subcooling values for small-volume and large-volume samples (Table 11); and (ii) the crystallisation onset ranges are shifted towards much higher temperatures. These two observations indicate that the nucleation of erythritol mainly takes place on the surface of the carbon foam (heterogeneous nucleation). On the one hand, heterogeneous nucleation is determined by the nucleation activity of the carbon foam surface and, therefore, it depends on the surface density of active sites for nucleation and on the specific surface area of the foam and not on the volume of erythritol. On the other hand, it is well known that a surface rich in nucleation sites decreases significantly the nucleation barriers and, therefore, reduces subcooling effects.

(a)



(b)

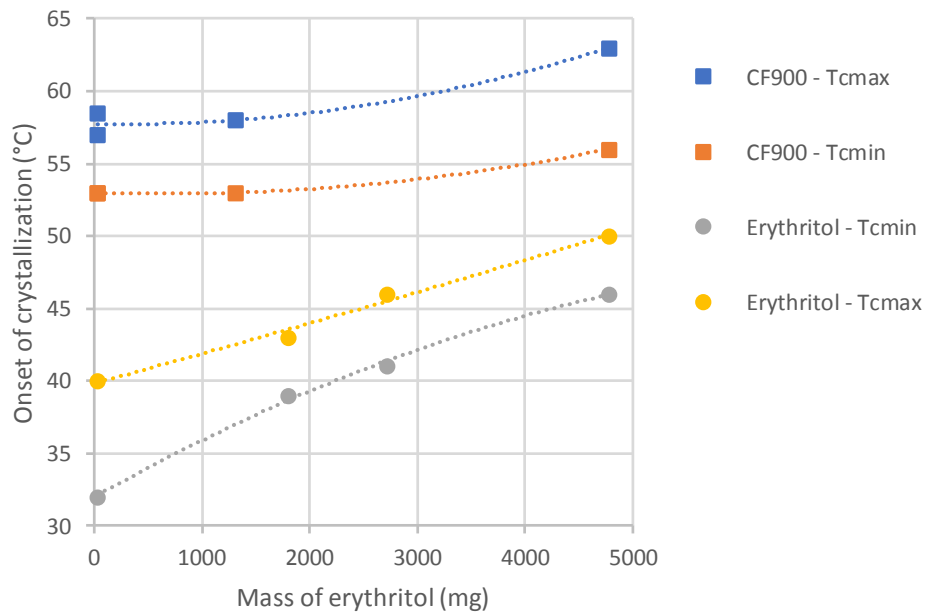


Figure 10. (a) DSC-thermograms (5 cycles) obtained for CF900-erythritol hybrid material (1305.53 mg of erythritol content) in large-volume DSC; (b) Upper and lower limits of the onset of crystallisation, as a function of the mass of the sample. Pure erythritol (circles) and CF900-erythritol hybrid material (squares).

Since the aforementioned results show that the sample volume has little influence on the nucleation outcomes, the tests on carbon-SA hybrid materials with hydrophobised carbon foams were carried out only in small-volume or large-volume DSC, depending on the volume of available samples. The crystallisation onset ranges observed during DSC testing are reported in Table 12.

Table 12. Results of DSC-testing of carbon-SA materials with hydrophobised carbon foams.

Hydrophobisation method	Sample Name	Mass of Erythritol (mg)	Onset of crystallisation range (°C)
Direct fluorination by molecular F ₂	CF _{0.02}	1514.53	{48.5, 56.5}
	CF _{0.07}	1163.31	{44, 46}
Grafting of perfluoroalkyl chains	pfdtms	2708.71	{48, 58}
Silanisation by grafting vinyltrimethoxysilane	vtmos	1795.05	{48, 52}
	ACN-CF ₃	29.77	{53, 58}
Electrochemical grafting of fluorinated moieties	ACN-CF ₅	29.30	{58, 60}
	H ₂ SO ₄ -CF ₃	29.53	{55, 58.5}
	H ₂ SO ₄ -CF ₅	29.92	{50, 56}

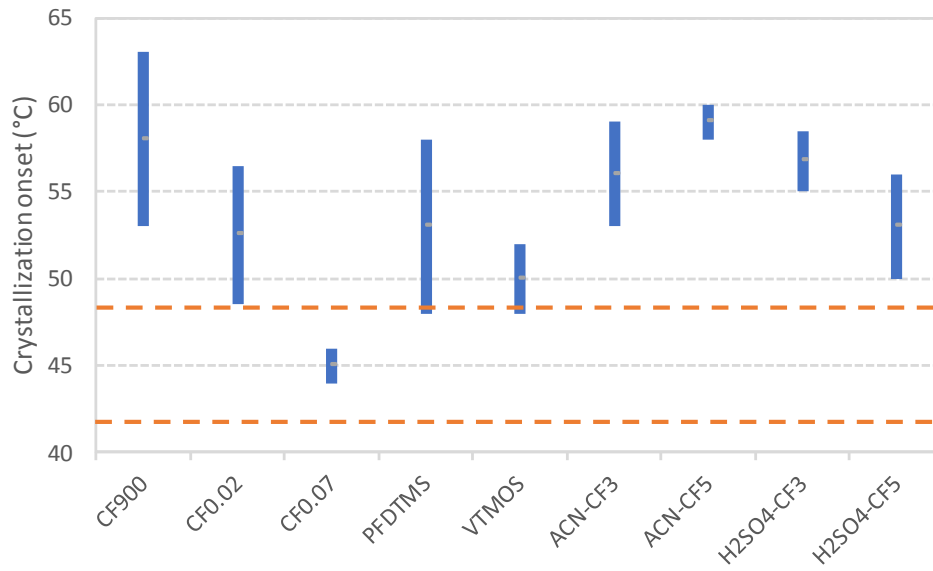
In Fig. 11(a), the crystallisation onset range of each carbon-SA hybrid material is represented by a vertical thick bar, whereas the onset crystallisation range of pure erythritol is displayed by horizontal dashed lines. It can be seen that all hydrophobised carbon-SA materials perform better than CF900, but only CF_{0.07} seems able to avoid completely heterogeneous nucleation. Indeed, the crystallisation onset range for CF_{0.07} lies within that of

pure erythritol. In order to rank hydrophobisation methods by their ability to prevent heterogeneous nucleation, the following efficiency indicator has been defined:

$$\eta = \min [1, (T_{CF900} - T)/(T_{CF900} - T_{ery})] \quad (3)$$

where T_{CF900} , T_{ery} and T represent the upper limits of the crystallisation onset ranges of CF900, of pure erythritol and of hydrophobised hybrid materials, respectively. The choice of the upper limits of the crystallisation interval in the definition of η (instead of the lower limits) is due to the fact that, for the application under consideration, it does not matter how deep the subcooling may be, but rather what is the minimum temperature that guarantees the absence of spontaneous crystallisation. According to Eq. (3), the efficiency indicator is $\eta \leq 0$ when $T \geq T_{CF900}$, which means that the hydrophobisation method does not work, the performance obtained being equal to ($\eta = 0$), or worse than ($\eta < 0$), that of CF900. Values such that $0 < \eta < 1$ correspond to $T_{ery} < T < T_{CF900}$: the higher the value of η , the closer the behaviour of the hybrid material is to that of erythritol ($\eta = 1$ for $T = T_{ery}$). The best possible result corresponds to hydrophobised foams without nucleation sites, so that the hybrid material behaves like pure erythritol. In such a case, $T \leq T_{ery}$ and the efficiency indicator is $\eta = 1$. It should be noted that T values below T_{ery} can only be observed due to the random nature of the nucleation process as is the case with sample CF_{0.02} (Fig. 11a). In other words, η values above 1 have no physical meaning. For this reason, the maximum value of the efficiency indicator was set to 1.

(a)



(b)

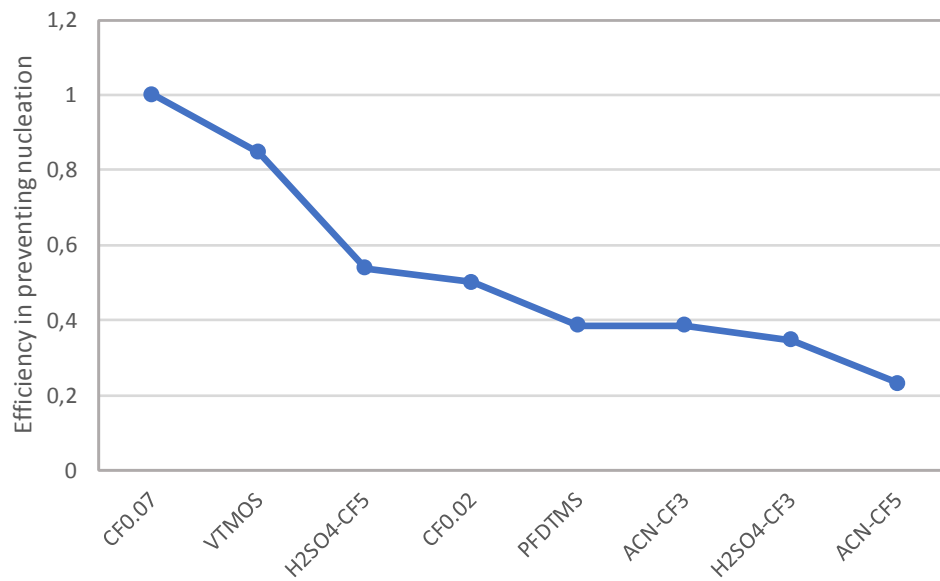


Figure 11. (a) Crystallisation onset ranges of carbon-SA hybrid materials; (b) Efficiency indicator in preventing nucleation of carbon-SA hybrid materials with hydrophobised carbon foams. Acronyms used in the X-axis are explained in Table 12. CF900 corresponds to the non-hydrophobised carbon foam

The efficiency indicator in preventing nucleation of the different hydrophobised carbon-SA material is displayed in Fig. 11(b). It can be seen that the most efficient sample in preventing nucleation is CF_{0.07} ($\eta = 1$), followed by the sample vtmos ($\eta = 0.85$). Samples CF_{0.02} and H₂SO₄-CF₅ show similar performances with η values close to 5. The worst performances correspond to samples pfdtms, ACN-CF₃, H₂SO₄-CF₃ and ACN-CF₅, whose efficiency indicator is less than 0.4.

Despite its widespread occurrence, mechanistic understanding of the role of a surface in heterogeneous nucleation still is limited. Nevertheless, to provide preliminary understanding of the results above, it is worth recalling the role of several factors, such as the surface chemistry and the surface morphology (especially porous structures: pore size and pore morphology), which might have great relevance in our context. In a first attempt to separate the contribution of these two factors to the nucleation kinetics, Daio et al. [57] proved that the surface chemistry influences the surface nucleation activity through interfacial free energies only, and they also revealed the importance of surface polarity on the nucleation activity of polar substances. The studies of Page and Sear [55,59] clearly demonstrated the important role of surface geometry on the nucleation behaviour. They found by Monte Carlo simulation of Lennard-Jones molecules that nucleation in nanoporous surfaces is orders of magnitude faster than on smooth surfaces, provided that the pores have a size close to that of the crystallites. They also showed that the nucleation in grooves formed by two intersecting planes is many orders of magnitude faster than on a flat surface. Moreover, when the wedge angle is the same as an intrinsic angle of the crystal, the nucleation rate reaches a maximum. The latter findings provide theoretical explanation for a common observation; that is, the beginning of crystallisation on edges, kinks and structural defects.

The nucleation results of the carbon-SA materials based on hydrophobised foams are next discussed considering the preceding remarks. As pointed out in section 3.1.1, regarding the direct fluorination method, fluorine first reacts with the most disordered carbon areas, such as edges of carbon layers and other structural defects, which are typically also the most active sites for nucleation. The nucleation activity of the foam surface is therefore reduced. This can explain the better ability to prevent nucleation shown by CF_{0.02} and CF_{0.07} compared to CF900. In addition, CF_{0.07}, with higher fluorine content, appears to provide greater reduction of structural defects and shows excellent nucleation prevention efficiency.

The vtmos sample also performs quite well, probably because (i) its specific surface area is significantly reduced compared to CF900 (Table 5); and (ii) the pore size distribution changes in the right way. Regarding this latter factor, it must be highlighted that samples CF900 and pfdtms present a significant number of pores narrower than 0.4 nm, whereas such small pores are not present in vtmos sample (Fig. 6). Likely, the pore size maximising the nucleation rate is less than 0.4 nm. The pfdtms sample behaves slightly better than CF900 but much worse than vtmos. The reason for this is probably that it has a lower surface area than CF900 but higher than vtmos in addition to pores narrower than 0.4 nm. The combined effect of micropores and low surface energy has indeed also been suggested for explaining the remarkable hydrophobicity of fluorinated activated carbon fibres [60].

For samples obtained by electrochemical grafting of fluorinated moieties, there is a quite good correlation between the amount of fluorine at the surface of the foam (Table 6, 3rd column) and the nucleation results (Table 12), which indicates that the ability of the carbon foam in preventing the nucleation of erythritol on its surface decreases as its fluorine content is increased. The best hydrophobisation methods that emerge from the initial screening carried out are, therefore, direct fluorination and silica deposition through silanisation.

Finally, yet importantly, it must be noticed that in none of the cases, neither the melting temperature nor the latent heat of erythritol were significantly modified by the presence of carbon surfaces (see Table 13). The latent heat of the erythritol confined into the carbon foam has been calculated as Q/m_{ery} , where m_{ery} is the mass of erythritol within the carbon foam (see Tables 11 and 12) and Q represents the energy of the peak of melting calculated from the DSC thermogram. The uncertainty values in Table 13 have been estimated from all experimental results available for each material (one or two samples, depending on the material, and 5 cycles of heating and cooling per sample). It can be seen that both the melting point and the latent heat of pure erythritol measured by DSC (118°C and 350 J g⁻¹, respectively) are always within the estimated uncertainty range.

Table 13. Melting temperature and estimated values of the latent heat of erythritol confined within the composite carbon foams.

Hydrophobisation method	Sample Name	Melting point (°C)	Latent heat of melting (J g ⁻¹)
None	CF900	117.5 ± 1.5	348 ± 17
Direct fluorination by molecular F ₂	CF _{0.02}	118.2 ± 1.0	343 ± 17
	CF _{0.07}	117.6 ± 1.0	351 ± 15
Grafting of perfluoroalkyl chains	pfdtms	118.2 ± 1.0	341 ± 19
Silanisation by grafting vinyltrimethoxysilane	vtmos	117.3 ± 1.0	345 ± 13
Electrochemical	ACN-CF ₃	118.1 ± 0.5	352 ± 10
	ACN-CF ₅	117.6 ± 0.5	347 ± 13

grafting of fluorinated moieties	H ₂ SO ₄ -CF ₃	118.0 ± 0.5	345 ± 15
	H ₂ SO ₄ -CF ₅	117.8 ± 0.5	349 ± 11

4. Conclusion

Hydrophobisation of sucrose-based carbon – graphite filler composite foams was carried out by four different techniques: (i) direct fluorination under a flow of hot molecular F₂; (ii) silanisation followed by heat treatment; (iii) chemical grafting of perfluoroalkyl chains; (iv) electrochemical grafting of trifluoro-methyl-benzene and pentafluoro-benzene. Whereas not all characterisation techniques could be systematically used, the enhanced hydrophobic character of treated samples could be observed, although to very different extents.

Direct fluorination was highly efficient from that point of view, but rather difficult to control because the resulting stoichiometry is hardly predictable. Silanisation was easier and the resultant hydrophobicity was only a little less than with the carbon foam fluorinated at the highest F stoichiometry. Grafting long perfluoroalkyl chains was also easy and quite efficient. Finally, electrochemical grafting led to very different results, depending on the nature of the diazonium salt and the solvent in which the synthesis was done. Overall, the final hydrophobicity was the combination of surface chemistry and roughness / microporosity.

Whatever the treatment, all carbon foams could be successfully impregnated with molten sugar alcohols, and the structure of the latter, once crystallised, was not influenced by the presence of the carbon host. The mechanical properties and the thermal conductivity of the hybrid materials based on sugar alcohol infiltrated in carbon foam were significantly higher than the pristine carbon foams. A very important point is that no surface treatment induced losses of either macroscopic porosity or thermal conductivity. The hydrophobised materials

thus fully retained their initial characteristics, making them relevant for solar thermal energy storage.

Moreover, DSC experiments clearly stated that neither the melting point nor the enthalpy of melting of the hosted phase-change material was modified by the presence of carbon surfaces, whether hydrophobised or not. Most importantly, the most hydrophobic carbon foams were able to induce a significant subcooling of the hosted phase-change material, which is an excellent feature for long-term, i.e., seasonal, heat storage. The carbon foam with stoichiometry $CF_{0.07}$ was the only material able to avoid completely heterogeneous nucleation of the sugar alcohol. A demonstrator is presently about to be built to prove the interest of hybrid materials based on carbon foam infiltrated by sugar alcohols for the seasonal storage of solar thermal energy. Several options for activating the crystallisation of the sugar alcohol on demand are being investigated and the most efficient one will be implemented in the demonstrator. In parallel, a thorough analysis of the thermal stability of the sugar alcohol is being carried out.

Acknowledgements

The research leading to these results has received funding from the European Community's Seventh Framework Programme (FP7/2007-2013) under grant agreement 296006. The authors also gratefully acknowledge the financial support of the CPER 2007-2013 "Structuration du Pôle de Compétitivité Fibres Grand'Est" (Competitiveness Fibre Cluster), through local (Conseil Général des Vosges), regional (Région Lorraine), national (DRRT and FNADT) and European (ERDF) funds, as well as the funding support received from the "Agencia Estatal de Investigación" of Spain (ref.: RTI2018-099557-B-C21).

References

- [1] R.K. Sharma, P. Gamesan, V.V. Tyagi, H.S.C. Metselaar, S.C. Sandaran, Developments in organic solid-liquid phase change materials and their applications in thermal energy storage, *Energ. Convers. Manag.* 92 (2015) 193-228.
- [2] K. Pielichowska, K. Pielichowski, Phase change materials for thermal energy storage, *Prog. Mat. Sci.* 65 (2014) 67-123.
- [3] M. Kenisarin, K. Mahkamov, Solar energy storage using phase change materials, *Renew. Sustain. Energy Rev.* 11 (2007) 1913-65.
- [4] M.M. Farid, A.M. Khudhair, S.A.K. Razack, S. Al-Hallaj, A review on phase change energy storage: materials and applications, *Energ. Convers. Manag.* 45(9–10) (2004) 1597–615.
- [5] A. De Gracia, L.F. Cabeza, Phase change materials and thermal energy storage for buildings, *Energy Build.* 103 (2015) 414–9.
- [6] A.M. Khudhair, M.M. Farid, A review on energy conservation in building applications with thermal storage by latent heat using phase change materials, *Energ. Convers. Manag.* 45(2) (2004) 263–75.
- [7] B. Zalba, J.M. Marín, L.F. Cabeza, H. Mehling, Review on thermal energy storage with phase change: materials, heat transfer analysis and applications, *Appl. Therm. Eng.* 23(3) (2003) 251–83.
- [8] L. Fan, J.M. Khodadadi, Thermal conductivity enhancement of phase change materials for thermal energy storage: A review, *Renew. Sustain. Energy Rev.* 15 (2011) 24–46.

- [9] H. Ji, D.P. Sellan, M.T. Pettes, X. Kong, J. Ji, L. Shi, R.S. Ruoff, Enhanced thermal conductivity of phase change materials with ultrathin-graphite foams for thermal energy storage. *Energy Environ. Sci.* 7 (2014) 1185-92.
- [10] T. Khadiran, M.Z. Hussein, Z. Zainal, R. Rusli, Encapsulation techniques for organic phase change materials as thermal energy storage medium: A review, *Sol. Energy Mater. Sol. Cells* 143 (2015) 78-98.
- [11] J.M. Khodadadi, L. Fan, H. Babaei, Thermal conductivity enhancement of nanostructure-based colloidal suspensions utilized as phase change materials for thermal energy storage: A review, *Renew. Sustain. Energy Rev.* 24 (2013) 418-44.
- [12] V. Canseco, Y. Anguy, J.J. Roa, E. Palomo, Structural and mechanical characterization of graphite foam/phase change material composites, *Carbon* 74 (2014) 266–81.
- [13] Z. Acem, L. Lopez, E. Palomo del Barrio, $\text{KNO}_3/\text{NaNO}_3$ -Graphite materials for thermal energy storage at high temperature: Part I. – Elaboration methods and thermal properties. *Appl. Therm. Eng.* 30 (2010) 1580–5.
- [14] Y. Zhong, S. Li, X. Wei, Z. Liu, Q. Guo, J. Shi, et al., Heat transfer enhancement of paraffin wax using compressed expanded natural graphite for thermal energy storage. *Carbon* 48(1) (2010) 300–4.
- [15] Y. Zhong, Q. Guo, S. Li, J. Shi, L. Liu, Heat transfer enhancement of paraffin wax using graphite foam for thermal energy storage, *Sol. Energy Mater. Sol. Cells* 94(6) (2010) 1011–4.
- [16] K. Lafdi, O. Mesalhy, A. Elgafy, Graphite foams infiltrated with phase change materials as alternative materials for space and terrestrial thermal energy storage applications, *Carbon* 46(1) (2008) 159–68.

- [17] O. Mesalhy, K. Lafdi, A. Elgafy, Carbon foam matrices saturated with PCM for thermal protection purposes, *Carbon* 44(10) (2006) 2080–8.
- [18] I. Kholmanov, J. Kim, E. Ou, R.S. Ruoff, L. Shi, Continuous carbon nanotube-ultrathin graphite hybrid foams for increased thermal conductivity and suppressed subcooling in composite phase change materials, *ACS Nano* 9(12) (2015) 11699-707.
- [19] P.F. Barret, B.R. Best, K.B. Oldham, Thermal energy storage in supersaturated salt solutions, *Mater. Chem. Phys.* 10 (1984) 39-49.
- [20] S. Hirano, T.S. Saitoh, M. Oya, M. Yamazaki, Long-term supercooled thermal energy storage. *AIAA* 2979 (2000) 1013-8.
- [21] B. Sanders, J. Rekstad, Supercooling salt hydrates: stored enthalpy as a function of temperature, *Sol. Energy* 80 (2006) 616-25.
- [22] A. Seppälä, K. Saari, M.J. Lampinen, Factors affecting supercooling of liquids from a heat storage perspective, *TKK Appl. Thermodynam.* 156 (2008) 1-58.
- [23] A. Godin, M. Duquesne, E. Palomo del Barrio, F. Achchaq, P. Monneyron, Bubble agitation as a new low-intrusive method to crystallize glass-forming materials, *Energy Procedia* 139 (2017) 352-7.
- [24] E. Palomo del Barrio, R. Cadoret, J. Daranlot, F. Achchaq, New sugar alcohols mixtures for long-term thermal energy storage applications at temperatures between 70°C and 100°C, *Sol. Energ. Mat. Sol. C.* 155 (2016) 454-68.
- [25] E. Palomo del Barrio, A. Godin, M. Duquesne, J. Daranlot, W. Alshaer, T. Kouadio, A. Sommer, Characterization of different sugar alcohols as phase change materials for thermal energy storage application, *Sol. Energ. Mat. Sol. C.* 159 (2017) 560-9.

- [26] P. Jana, E. Palomo del Barrio, V. Fierro, G. Medjahdi, A. Celzard, Design of carbon foams for seasonal solar thermal energy storage, *Carbon* 109 (2016) 771-87.
- [27] A. Shukla, D. Buddhi, R.L. Sawhney, Thermal cycling test of few selected inorganic and organic phase change materials. *Renewable Energy* 33 (2008) 2606–2614.
- [28] A. Kaizawa, N. Maruoka, A. Kawai, H. Kamano, T. Jozuka, T. Senda, T. Akiyama, Thermophysical and heat transfer properties of phase change material candidate for waste heat transportation system. *Heat Mass Transfer* 44 (2008) 763–769.
- [29] S. Neidermaier, Sugar alcohol-based materials for seasonal storage applications – Thermal stability, Final workshop and on-site demonstration of FP/ SAM.SSA project, March 17-18, 2015, Vitoria-Gasteiz, Spain (available on-line: <http://www.samssa.eu/>).
- [30] F. Cosnier, A. Celzard, G. Furdin, D. Bégin, J.F. Marêché, O. Barrès, Hydrophobisation of active carbon surface and effect on the adsorption of water, *Carbon* 43 (2005) 2554-63.
- [31] C. Delgado-Sánchez, M. Letellier, V. Fierro, H. Chapuis, C. Gérardin, A. Pizzi, A. Celzard, Hydrophobisation of tannin-based foams by covalent grafting of silanes, *Ind. Crop Prod.* 92 (2016) 116-26.
- [32] L. Wang, Y. Zhao, K. Lin, X. Zhao, Z. Shan, Y. Di, et al., Super-hydrophobic ordered mesoporous carbon monolith, *Carbon* 44 (2006) 1298–352.
- [33] A. Chaussé, M.M. Chehimi, N. Karsi, J. Pinson, F. Podvorica, C. Vautrin-UI. The Electrochemical Reduction of Diazonium Salts on Iron Electrodes. The Formation of Covalently Bonded Organic Layers and Their Effect on Corrosion, *Chem. Mater.* 14 (2002) 392-400.

- [34] E.W. Washburn, The dynamics of capillary flow. *Physical review* 17 (1921) 273.
- [35] H. Zhang, M. Duquesne, A. Godin, S. Niedermaier, E. Palomo del Barrio, S.V. Nedeia, C.C. Rindt, Experimental and in silico characterization of xylitol as seasonal heat storage material. *Fluid Phase Equilibria*, *Fluid Phase Equilibria* 436 (2017) 55-68.
- [36] W. Zhang, M. Dubois, K. Guérin, P. Bonnet, E. Petit, N. Delpuech, et al., Effect of graphitization on fluorination of carbon nanocones and nanodiscs, *Carbon* 47(12) (2009) 2763–75.
- [37] J. Giraudet, M. Dubois, K. Guérin, C. Delabarre, A. Hamwi, F. Masin, Study of the post-fluorination of $(C_{2.5}F)_n$ fluorine-GIC, *J. Phys. Chem. B* 111 (2007) 14143–51.
- [38] A. Panich, Nuclear magnetic resonance study of fluorine– graphite intercalation compounds and graphite fluorides, *Synth. Met.* 100 (1999) 169–85.
- [39] T. Mallouk, B.L. Hawkins, M.P. Conrad, K. Zilm, G.E. Maciel, N. Bartlett, Raman, infrared and n.m.r. studies of the graphite hydrofluorides $C_xF_{1-\delta}(HF)_\delta$ ($2 \leq x \leq 5$), *Philos. Trans. R. Soc. London. Ser. A.* 314 (1985) 179-83.
- [40] M. Dubois, J. Giraudet, K. Guérin, A. Hamwi, Z. Fawal, P. Pirotte, at al., EPR and Solid-State NMR Studies of Poly(dicarbon monofluoride) $(C_2F)_n$, *J. Phys. Chem. B* 110 (24) (2006) 11800-8.
- [41] J. Giraudet, M. Dubois, K. Guérin, C. Delabarre, A. Hamwi, F. Masin, F., Solid-State NMR (^{19}F and ^{13}C) Study of Graphite Monofluoride $(CF)_n$: ^{19}F Spin–Lattice Magnetic Relaxation and $^{19}F/^{13}C$ Distance Determination by Hartmann–Hahn Cross Polarization, *J. Phys. Chem. B* 109 (1) (2005) 175-81.

- [42] M. Dubois, K. Guérin, J.P. Pinheiro, F. Masin, Z. Fawal, A. Hamwi, A. NMR and EPR studies of room temperature highly fluorinated graphite heat-treated under fluorine atmosphere, *Carbon* 42 (2004) 1931-40.
- [43] K. Guérin, J.P. Pinheiro, M. Dubois, Z. Fawal, F. Masin, R. Yazami, A. Hamwi, Synthesis and characterization of highly fluorinated graphite containing sp^2 and sp^3 carbon, *Chem. Mater.* 16 (2004) 1786-92.
- [44] Y. Sato, K. Itoh, R. Hagiwara, T. Fukunaga, Y. Ito, On the so-called “semi-ionic” C-F bond character in fluorine-GIC, *Carbon* 42 (2004) 3243-9.
- [45] K. S. W. Sing, D. H. Everett, R. A. W. Haul, L. Moscou, R. A. Pierotti, J. Rouquerol, et al., Reporting Physisorption Data for Gas/Solid Systems with Special Reference to the Determination of Surface Area and Porosity, *Pure Appl. Chem.* 57(4) (1985) 603-19.
- [46] M. Zayat, D. Davidov, H. Selig, Fluorination of carbon fibers by halogen fluorides, *Carbon* 32 (3) (1994) 485-91.
- [47] K.K.C. Ho, G. Beamson, G. Shia, N.V. Polyakova, A. Bismarck Surface and bulk properties of severely fluorinated carbon fibres, *J. Fluor. Chem.* 128 (11) (2007) 1359-68.
- [48] K.K.C. Ho, A.F. Lee, A. Bismarck, Fluorination of carbon fibres in atmospheric plasma, *Carbon* 45 (4) (2007) 775-84.
- [49] L. Wang, Y. Zhao, K. Lin, X. Zhao, Z. Shan, Y. Di, et al. Super-hydrophobic ordered mesoporous carbon monolith. *Carbon* 44 (2006) 1336-9.
- [50] M. Fuji, M. Araki, T. Takei, T. Watanabe, M. Chikazawa, Structure and wettability of various silica surfaces: evaluation on the nano and macro levels, *Kona* 18 (2000) 236-41.

- [51] K.C. Park, H.J. Choi, C.H. Chang, R.E. Cohen, G.H. McKinley, G. Barbastathis, Nanotextured Silica Surfaces with Robust Superhydrophobicity and Omnidirectional Broadband Supertransmissivity, *ACS Nano* 6 (5) (2012) 3789-99.
- [52] A. Cassie, S. Baxter, Wettability of porous surfaces, *Trans. Faraday Soc.*, 40 (1944) 546-51.
- [53] R.N. Wenzel, Resistance of solid surfaces to wetting by water, *Ind. Eng. Chem.*, 28 (1936) pp. 988-94.
- [54] L.J. Gibson, M.F. Ashby, *Cellular Solids: Structure and Properties*, second ed., Cambridge Solid State Press, Cambridge University Press, 1997.
- [55] A.J. Page, R.P. Sear, Heterogeneous nucleation in and out of pores, *Phys. Rev. Lett.* 97 (2006) 065701.
- [56] D. Frenkel. Seeds of phase change. *Nature* 443 (7112) (2006) 641.
- [57] Y. Diao, A.S. Myerson, T.A. Hatton, B.L. Trout, Surface design for controlled crystallization: The role of surface chemistry and nanoscale pores in heterogeneous nucleation, *Langmuir* 27(9) (2011) 5324-34.
- [58] D. Kashchiev, *Nucleation: basic theory with applications*; Butterworth Heinemann: Oxford, Boston, 2000.
- [59] A.J. Page, R.P. Sear. Crystallization controlled by the geometry of a surface, *J. Am. Chem. Soc.* 131 (2000) 17550-1.
- [60] H. Touhara, F. Okino, Property control of carbon materials by fluorination. *Carbon* 2000; 38(2) 241-67.